UNIVERSITÄT HAMBURG

Commissioning of an Electro-Optic Electron Bunch Length Monitor at FLASH

Diplomarbeit
von
Jonas Breunlin

vorgelegt dem
Fachbereich Physik der Universität Hamburg

angefertigt am
Deutschen Elektronen Synchrotron (DESY), Hamburg

Hamburg, März 2011

Gutachter: Prof. Dr. Jörg Roßbach (Universität Hamburg)
P.D. Dr. Bernhard Schmidt (Deutsches Elektronen Synchrotron)

Jonas Breunlin
Institut für Experimentalphysik
Universität Hamburg
Notkestraße 85
22607 Hamburg
E-Mail: jonas.breunlin@desy.de

Dieses Dokument wurde mit LaTeX und KOMA-Script erstellt.

Erklärung zur Eigenständigkeit

Hiermit versichere ich, daß ich die vorliegende Diplomarbeit selbständig verfaßt und - einschließlich beigefügter Abbildungen, Skizzen und Diagramme - keine anderen als die im Literaturverzeichnis angegebenen Quellen, Darstellungen und Hilfsmittel benutzt habe. Diese Arbeit lag noch keiner anderen Person oder Prüfungsbehörde im Rahmen einer Prüfung vor. Mit dem späteren Ausleihen meiner Arbeit bin ich einverstanden.

Jonas Breunlin - Hamburg, den 21. März 2011

Abstract

The demands on the electron beam qualities for free-electron lasers (FEL) are challenging in terms of high peak currents. At FLASH, the high-gain FEL in Hamburg, longitudinal bunch compression is performed to achieve the requested high charge densities in short bunches. The precise control of the bunch compression process requires advanced diagnostics on the longitudinal bunch profile.

The bunch length monitor presented in this thesis is based on a non-destructive detection using the electro-optic effect. The focus is on a compact and reliable system for permanent bunch diagnostics. The monitor provides single-shot measurements of the longitudinal bunch profiles with lengths of a few picoseconds by spectrally encoding their charge distribution.

First measurements for characterization purpose have been performed. It has been shown that the monitor is suitable for monitoring the longitudinal bunch profile behind the first bunch compressor at FLASH. Electron bunch profiles with slopes corresponding to a full width half maximum of about 1.4 ps have been detected. That is the intrinsic resolution limit of the utilized method.

Zusammenfassung

Die Anforderungen an die Elektronenstrahleigenschaften von Freie-Elektronen-Lasern (FEL) bezüglich hoher Spitzenströme sind anspruchsvoll. Bei FLASH, dem hochverstärkenden FEL in Hamburg, wird eine longitudinale Kompression der Elektronenpakete durchgeführt, um die geforderten hohen Ladungsdichten bei kurzen Elektronenpaketen zu erreichen. Die präzise Kontrolle der Elektronenpaketkomprimierung bedarf hochentwickelter Diagnostik des longitudinalen Profils.

Der Elektronenpaketlängenmonitor, der in dieser Arbeit vorgestellt wird, basiert auf der zerstörungsfreien Detektion mittels des elektro-optischen Effekts. Der Schwerpunkt liegt auf einem kompakten und zuverlässigen System zur durchgehenden Untersuchung der Elektronenpakete. Der Monitor bietet Einzelschußmessungen longitudinaler Elektronenpaketprofile mit Längen von einigen Pikosekunden durch eine spektrale Kodierung der Ladungsverteilung.

Erste Messungen sind zum Zweck der Systemcharakterisierung durchgeführt worden. Es stellte sich heraus, daß der Monitor zur Überwachung des longitudinalen Elektronenpaketprofils hinter dem ersten Elektronenpaketkompressor geeignet ist. Elektronenpaketprofile mit Steigungen, die einer Halbwertsbreite von etwa 1.4 ps entsprechen, sind gemessen worden. Dies stellt die intrinsische Grenze des Auflösungsvermögens der verwendeten Methode dar.

Contents

List of Figures

Introduction

Light pulses of high intensity with wavelengths in the X-ray regime and ultra-short pulse durations allow for experiments with spatial resolutions in the atomic range and on femtosecond time scales. Studies on single atoms as well as on biological macro-molecules can be performed, affecting sciences like physics, chemistry and biology. Linear accelerator driven free-electron lasers (FEL) are capable of producing light pulses with wavelengths in the vacuum ultraviolet (VUV) and X-ray range with a high peak brilliance. FLASH, the Free-electron LASer in Hamburg, the Linear Coherent Light Source (LCLS) and the projected European XFEL are high-gain FELs, based on self-amplified spontaneous emission (SASE). The excitation and amplification of X-radiation are accomplished in a single passage of the electron driving beam through magnetic structures, the undulators.

For an optimization of the SASE process in the undulators, the demands on the electron beam in terms of emittance and peak currents are very high. The required peak currents of several kiloampere and electron bunch lengths of a few 10 femtoseconds can not be produced at the point of injection but must be achieved by longitudinal bunch compression in the accelerator. With an interaction of accelerating structures and magnetic chicanes, the bunch compressors, the longitudinal bunch profile can be shaped. Sophisticated diagnostics is required to obtain precise knowledge of the longitudinal bunch profile. This is essential for the control and stabilization of the bunch compression and the SASE process.

The diagnostic tools must allow bunch profile measurements down to sub-picosecond resolutions. Only a few techniques are suitable for the required online diagnostics. Spectroscopy of coherent transition radiation (CTR) [1] and coherent diffraction radiation (CDR) [2] is an established technique, enabling bunch profile measurements in an indirect way. The transverse deflecting structure (TDS) [3] is a powerful tool with a resolution down to a few 10 femtoseconds at the cost of a complex infrastructure and much beam pipe space.

Diagnostic devices probing the electric field of a bunch with the electro-optic (EO) effect offer bunch length information in a non-destructive way. This has first been shown in an electron accelerator using a scanning technique [4]. Single-shot operation can be achieved as well using a spectrally resolving method (EOSD) [5], a temporally resolving method (EOTD) [6] or the spatially resolved electro-optic detection [7]. Bunch length measurements with a resolution below 60 fs have been achieved [8]. Nevertheless, all experiments

done have been done as proof-of-principle experiments or for a dedicated, singular purpose. No electro-optic bunch length monitor for routine operation has been established so far.

This thesis deals with the setup and commissioning of an electro-optic monitor system at FLASH. It is located behind the first bunch compressor, 30 m downstream of the electron injector. This position is chosen to measure the longitudinal bunch profile at an early stage in the electron accelerator. Especially since a third harmonic system for the linearization of the longitudinal phase space is in operation, it is reasonable to study the bunch compression process with a monitor located on this spot.

The monitor system provides single-shot detection based on electro-optic spectral decoding (EOSD). Non-destructive measurements of the longitudinal bunch profile can be performed allowing for a permanent diagnostics. The system is designed as a prototype of a compact diagnostic tool with a focus on a robust setup and a high reliability. Furthermore, the requirements regarding the electron beam pipe length and the local infrastructure are reduced to a minimum. Similar monitors are planned to be used for diagnostics purposes in the European XFEL.

This thesis is divided into six chapters, beginning with a brief description of the FLASH accelerator with focus on the longitudinal bunch shaping and diagnostics. In chapter 2 the basics of electro-optic detection are discussed. In chapter 3 and 4 a description of the experimental setup is given, followed by a characterization of the particular components. The process of the EO data evaluation is discussed in chapter 5. The EO measurements for the monitor commissioning as well as first comparative studies on the bunch arrival-time and the longitudinal bunch profile are presented in chapter 6.

1 Longitudinal Bunch Shaping and Diagnostics at FLASH

FLASH is the free-electron laser at DESY in Hamburg. It started as the TESLA Test Facility (TTF) in the context of the 500 GeV linear collider project TESLA. Meanwhile TESLA has been evolved into the International Linear Collider (ILC) project. Based on this superconducting electron accelerator, a high-gain free-electron laser has been built with numerous upgrades over several years. FLASH produces femtosecond light pulses in the UV and soft X-ray regime in a single undulator pass due to self-amplified spontaneous emission (SASE) [9]. Since the latest upgrade in winter 2009 the maximum beam energy achieved is 1.2 GeV. The minimum wavelength of the radiation produced is 4.12 nm.

The linear accelerator section of FLASH consists of an electron photoinjector, seven accelerating modules (ACC), two bunch compressors (BC) and numerous diagnostic stations. It has a length of about 200 m and is followed by the undulator section. See figure 1.1 for a schematic overview of the machine. During the last upgrade a third harmonic system (ACC39) for phase space linearization has been installed and is in routine operation. The new EO monitor presented in this thesis installed behind the first bunch compressor BC2.

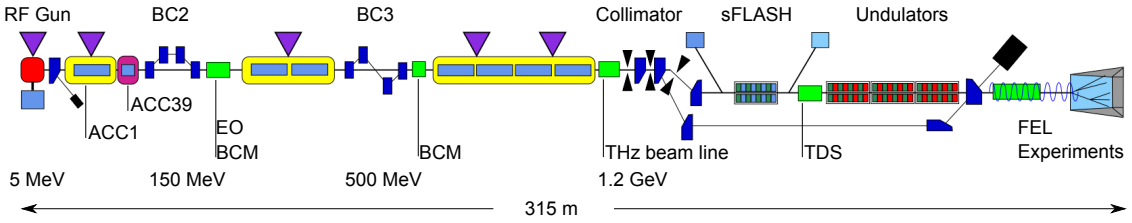

Figure 1.1: Overview of the FLASH facility after the upgrade in 2009. Adapted from [10].

1.1 Longitudinal Bunch Shaping

1.1.1 Accelerating Modules

The accelerating modules are based on the superconducting TESLA cavities, made of niobium and cooled to superfluid helium temperatures [11]. An accelerating module consists of

eight niobium resonators, each resonator has nine cells. In the cavities an electro-magnetic wave is excited in a TEM_{010}-mode, providing longitudinal electric fields (Fig. 1.2). The dimension of the TESLA structure is chosen in a way to let relativistic electrons traverse one cell in half a period of the driving frequency of 1.3 GHz and passing the waist between two cells during a zero-crossing of the accelerating electric field. An energy gain of more than 150 MeV can be achieved in a module.

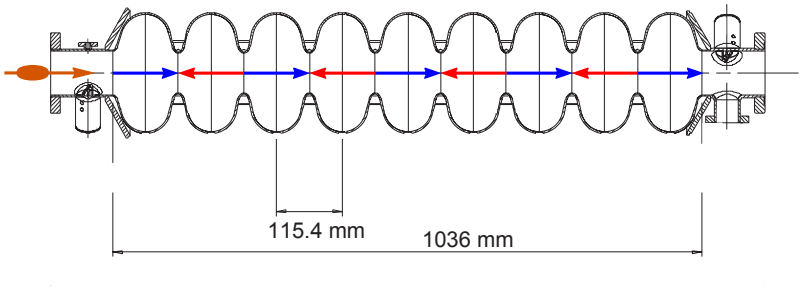

Figure 1.2: Schematic of a TESLA structure. The alternating longitudinal electric fields accelerate the electron bunch (orange). Adapted from [11].

The phase of the sinusoidal electric field at the moment the electron bunch passes the center of a cell, Φ_{ACC}, is crucial (Fig. 1.3). For $\Phi_{ACC} = 0$ the maximum electric field V_{ACC} is reached and, therefore, the acceleration is maximized. Under this so called on-crest condition the energy gain in an accelerating module is ΔE_{ACC}. Using the sinusoidal characteristic of the accelerating field, an energy chirp can be applied on the electron bunch. Therefore, the injection phase can be set off-crest ($\Phi_{ACC} \neq 0$). For $\Phi_{ACC} > 0$, for example, the slope of the accelerating field leads to a higher energy gain for electrons in the tail of the bunch than for those in the head. The energy chirp is a requirement for the longitudinal bunch compression. Considering the sinusoidal shape of the accelerating field, the energy chirp is not linear.

1.1.2 Third Harmonic System

The third harmonic system (ACC39) is a superconducting accelerating module driven at the third harmonic frequency of the TESLA stuctures, that means 3.9 GHz. The third harmonic system enables increased control of the longitudinal phase space due to a higher curvature of the accelerating field achieved by the higher driving frequency. The parameters Φ_{ACC39} and ΔE_{ACC39} define the operation state of the 3rd harmonic system according to the TESLA structures. The combination of ACC1 and ACC39 allows for a linerization of the longitudinal phase space (energy chirp) which is an improvement for the bunch compression process.

1.1.3 Bunch Compressors

The longitudinal compression is necessary because charge densities, needed for the FEL process, can not be produced directly in a photoinjector gun. Repulsive forces between the electrons would lead to dramatic increase of the transverse emittance of the electron bunch [9]. Since the space charge effects decrease with $1/\gamma^2$, a two step acceleration and compression scheme is favourable. The electron linear accelerator at FLASH is equipped with two bunch compressors. The first is located behind the third harmonic system ACC39 and is called BC2 for historical reasons. It compresses the electron bunch from the gun, having a length of approx. 3 mm (corresponding to 10 ps at highly relativistic velocities) by a factor of 5 to 10.

In a bunch compressor electrons traverse a magnetic chicane made of four deflecting dipole magnets (Fig. 1.3). The angle of deflection depends on the relativistic γ and, therefore, the path length through the bunch compressor is momentum dependent. Electrons with a higher momentum, i.e. higher energetic electrons, traverse the bunch compressor on a shorter path than lower energetic ones. If those electrons are in the tail of the electron bunch, they can catch up with the leading part, leading to a longitudinal compression of the bunch.

The energy chirp of the electron bunch applied in ACC1 and ACC39 with a combination of the parameters Φ_{ACC} and ΔE_{ACC} determines the longitudinal bunch profile produced in BC2.

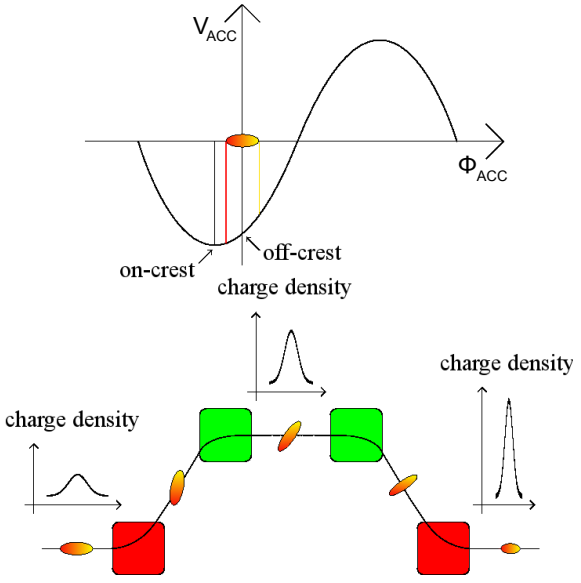

Figure 1.3: Illustration of the longitudinal bunch compression. By courtesy of C. Behrens.

1.1.4 Time Structure

The resistive losses in a superconducting cavity are very small. This leads to a very high quality factor which is higher than $2 \cdot 10^{10}$ for an unloaded TESLA cavity [11]. At FLASH the electric field in which electron bunches are accelerated can be sustained for up to 800 µs (Fig. 1.4b)). Usually up to 800 bunches separated by 1 µs can be accelerated in a sequence called bunch train. In the usual operation mode the bunch train repetition rate is 10 Hz.

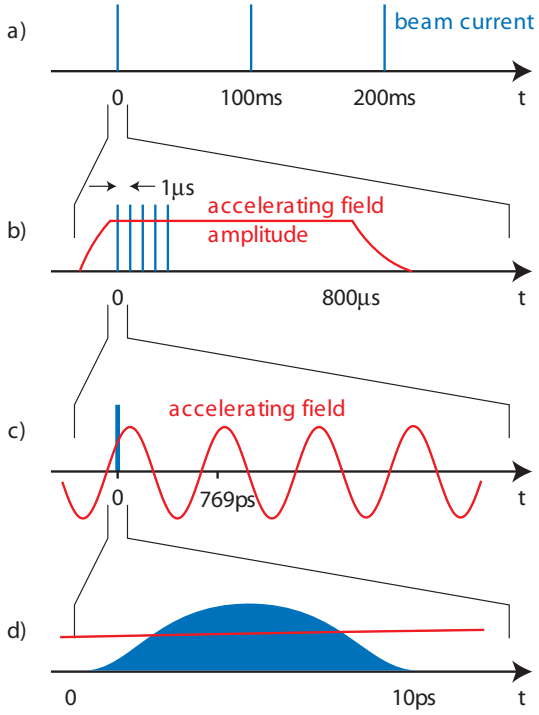

Figure 1.4: The FLASH time structure. a) Pulse trains at 10 Hz repetition rate. b) A bunch train accelerated by the flat top of the electric field envelope. c) A single bunch and the accelerating field with a frequency of 1.3 GHz. d) A Gaussian electron bunch with a FWHM of 5 ps. The drawings are not to scale. Adapted from [12].

1.2 Longitudinal Diagnostics

Principles of the longitudinal bunch diagnostics based on transverse deflection and on coherent radiation are presented in this section. A detailed description of the diagnostics method based on the electro-optic effect can be found in the next chapter.

1.2.1 Transverse Deflecting Structure

In a transverse deflecting structure (TDS) the temporal profile of an electron bunch is transformed to a transversal profile by a rapidly changing electro-magnetic field. This is

similar to the operation principle of an oscilloscope.

Electrons are injected into the deflecting cavity at the zero-crossing of the oscillating electro-magnetic field. This leads to a varying transverse deflection along the z-coordinate but no net-deflection of the bunch. A fast kicker magnet directs the bunch to a screen to excite optical transition radiation (OTR). The radiation produced is detected by a camera. The short fill time of the cavity and the fast kicker provide the diagnostics of a single bunch in a 1 MHz bunch train while leaving the other bunches unaffected. Longitudinal diagnostics at free-electron lasers using a TDS has first been done at SLAC [3]. A similar system with a lengths of 3.6 m and a frequency of 2.865 GHz has been installed in the FLASH accelerator (Fig. 1.1). A time resolution below 10 fs has been reached with an adapted accelerator beam optics whereas about 30 fs are achievable under FEL operation conditions [13].

The transverse deflection applied in the cavity prohibits a further utilization of the bunch for diagnostics or the FEL process which makes the TDS a destructive method. Besides the beam line length of more than 3 m, the infrastructure needed to operate a TDS includes a megawatt klystron to supply the cavity and a kicker magnet.

1.2.2 Coherent Radiation Diagnostics

Coherent radiation of electron bunches can be observed if the bunch traverses a screen, emitting coherent transition radiation (CTR) or a slit, emitting coherent diffraction radiation (CDR). Sub-picosecond bunch lengths produce radiation in the THz regime that is used for longitudinal diagnostics. The influence on the electron bunch is very small using CDR, thus tools utilizing this diagnostic method can be viewed as non-destructive.

A bunch compression monitor (BCM) based on CDR is installed behind each of the two bunch compressors at FLASH [14]. The electron beam traverses a 5 mm (BCM behind BC2) slit in a screen that is fixed in the beam pipe under an angle of 45 °. The diffraction radiation produced is coupled out and detected by a broadband pyro detector. The measured signal amplitude integrated over a wavelength interval from 80 µm to 3 mm depends on the electron bunch compression. The BCM system is a fast device for bunch length measurements and can be used in the beam-based feedback for the phase stabilization of the accelerating modules within a bunch train. As a consequence of the non-spectral resolving detection scheme, the temporal resolution of the bunch profile is not possible.

The THz spectroscopy is a more complex approach. The knowledge of the spectral intensity distribution of the THz radiation allows a reconstruction of the charge distribution in time domain though the phase information is lost in the measurement. The extremely broadband radiation produced requires a cascade of optical gratings and multichannel de-

tectors to cover a wide spectral range. The investigation of CTR with a THz spectrometer at FLASH obtained frequency components that correspond to bunch shape features as short as 15 fs [15]. FLASH provides a THz beamline [16] (Fig. 1.1) and a laboratory at the end of the linear accelerator section where a THz spectroscopy setup is in preparation.

2 Electro-Optic Diagnostics

2.1 Principles of Signal Detection

The electro-optic (EO) diagnostics allows for the detection of the transient electric field of a relativistic electron bunch passing an electro-optic crystal at close distance. The birefringence induced in the crystal is probed by a laser pulse providing an image of the transient electric field.

2.1.1 Relativistic Electron Bunches

For a highly relativistic charge the longitudinal component of the Coulomb field E_z is suppressed by a factor $1/\gamma$ with respect to the radial component E_r [17]. The radial component of the electric field of a point charge Q, moving at a constant speed $v = \beta c$ along the z-axis is given by

$$E_{r,Q}(r,t) = \frac{Q}{4\pi\epsilon_0} \cdot \frac{\gamma r}{(r^2 + \gamma^2 v^2 t^2)^{3/2}} \ , \tag{2.1}$$

assuming that the charge is at $z = 0$ at time $t = 0$.

The charge distribution of an electron bunch can be described as a line charge along the z-axis with a homogeneous charge distribution in a first approximation. The Coulomb field of a relativistic line charge can be derived from equation 2.1. With the line charge length l_B and charge q observed at a radial distance r it is

$$E_r(r) = \frac{\gamma q}{2\pi r \epsilon_0} \cdot \sqrt{\frac{1}{4r^2 + (\gamma^2 - 1)\, l_\mathrm{B}^2}} \tag{2.2}$$

at the maximum field. This yields an E_r proportional to $1/r$ for highly relativistic line charges and if

$$r < \frac{l_\mathrm{B}\gamma}{2} \tag{2.3}$$

for the radial distance r to the observer. For $\gamma = 300$ and a bunch length $l_\mathrm{B} = 0.3\,\mathrm{mm}$, which are typical beam parameters behind BC2 at FLASH, the radial distance r to the observer should not exceed 4.5 cm.

2.1.2 Pockels Effect

Gallium phosphide (GaP) is an electro-optic crystal material that is not intrinsically birefringent. Birefringence is induced at presence of an electric field, that means the material develops different refractive indices along two crystal axes, which are perpendicular to each other. Affecting the phase velocity of an electro-magnetic wave, the crystal axes may be denoted with n_s and n_f, $n_\mathrm{s} > n_\mathrm{f}$ for the slow and fast axis, respectively. The dominating effect causing birefringence in GaP is the linear electro-optic effect, called the Pockels effect.

The Coulomb field of a highly relativistic electron bunch with sub-millimeter (corresponding to a few picoseconds) of length passes the EO crystal at a close distance. This corresponds to a half-cycle electric THz pulse impinging on the crystal.

The electric field is radially polarized. For the distance between the crystal and the electron bunch and the small region probed by the laser pulse a linear polarization can be assumed. The birefringence induced depends on the spatial orientation of the polarization vector and the distinguished crystal axes [18].

2.1.3 Phase Retardation

A polarized laser pulse is sent through the EO crystal to probe the induced birefringence (Fig. 2.1). The effect on the laser pulse depends on the orientation of its polarization vector relative to the slow axis and the fast axis of the crystal. Entering the crystal, the polarization vector decompounds into two orthogonal components, each propagating with the phase velocity given by the refractive index of the distinguished crystal axis. The result is the phase retardation Γ between the two orthogonal components of the laser field. The phase retardation can be maximized if the laser polarization has an angle of $45\,^\circ$ to the slow axis and the fast axis.

Γ depends on the crystal thickness d and is proportional to the electric field E_THz for the Pockels effect. The Pockels coefficient r_{41} and n_0 are material properties and ω is the angular frequency of the laser. For a crystal orientation leading to maximal phase retardation we obtain [18]

$$\Gamma_\mathrm{max} = \frac{n_0^3\, r_{41}\, E_\mathrm{THz}\, \omega}{c}\, d\,. \tag{2.4}$$

A phase retardation turns the polarization of the initially linear polarized laser beam elliptically when traversing the crystal.

2.1.4 Detection Schemes

The modulation of the polarization of the laser pulse contains an information on the probed THz pulse. A transformation of the polarization modulation into an intensity modulation

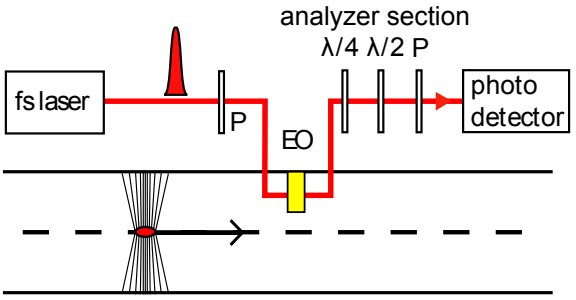

Figure 2.1: Schematic of a setup for electro-optic bunch diagnostics. Adapted from [19].

enables an easier transport through optical fibers and it can be detected for example by a photodiode or a camera. This is achieved in the analyzer section.

The analyzer section consists of a quarter-wave retarder for compensation of birefringence, which means it turns the polarization of the light linear. The orientation of the polarization can be influenced by a half-wave retarder. A polarizing beam splitter separates the incoming laser pulse into two components with perpendicular polarization axes. In combination with the half-wave retarder, this results in a transmission that depends on the polarization orientation of the incoming light. The analyzer section allows for multiple detection schemes [19].

In the *crossed polarizer setup*, both retarders are used to turn the polarization of the laser perpendicular to the polarization transmitted by the polarizer (crossed polarizer) and, therefore, minimize the signal on the detector. In this thesis, the angles for the quarter-wave retarder and the half-wave retarder are denoted as $\Phi = 0$ and $\Theta = 0$, respectively, in the *crossed polarizer setup*. A phase retardation Γ causes an intensity on the detector $I_{\mathrm{det,CP}}$, depending on the initial laser intensity I_{las}

$$I_{\mathrm{det,CP}} = I_{\mathrm{las}} \sin^2\left(\frac{\Gamma}{2}\right) \ . \tag{2.5}$$

The detected intensity depends quadratically on E_{THz} (Eq. 2.4), assuming $\Gamma \ll 1$. The transmission through the analyzer section is very low for methodical reasons and is, in theory, zero at the absence of induced birefringence. In praxis the detector noise and imperfections of the optical components and of the alignment decrease the signal-to-noise ratio.

In the *near crossed polarizer setup* the half-wave retarder angle Θ is turned by a few degrees. The signal intensity on the detector is

$$I_{\mathrm{det}} = \frac{I_{\mathrm{las}}}{2}\left[1 - \cos\left(\Gamma + 4\,\Theta\right)\right] \ . \tag{2.6}$$

It obtains a higher intensity level on the detector which increases the signal-to-noise ratio

compared to the *crossed polarizer setup*. I_{det} is proportional to E_{THz} and is sensitive to the sign of the electric field. Resolving equation 2.6 to the phase retardation Γ yields

$$\Gamma = \arccos\left(1 - 2\,\frac{I_{\mathrm{det}}}{I_{\mathrm{las}}}\right) - 4\,\Theta\ . \tag{2.7}$$

For the monitor commissioned the *near crossed polarizer setup* is chosen. The optimum of the half-wave retarder angle Θ must be found experimentally.

2.2 Diagnostic Methods

The electro-optic detection can be used to sample the temporal structure of the Coulomb field of an electron bunch. Several techniques have been developed based on scanning or single-shot detection. The principles of the signal detection including the detection schemes introduced in the previous section are applied in three of the four methods discussed in this section. An exception is the spatial decoding method with a non-collinear propagation of the THz pulse and the laser pulse through the EO crystal. The drawings in this section are adapted from [19].

2.2.1 Electro-Optic Sampling

One simple method for electro-optical bunch measurements is the sampling technique (EOS). A short laser pulse with a variable delay probes the THz pulses of many electron bunches in slices and is detected with a photodiode (Fig. 2.2). An averaged longitudinal bunch profile is obtained. This has been the first electro-optic diagnostic method established [4]. The temporal resolution limit is determined by the laser pulse length.

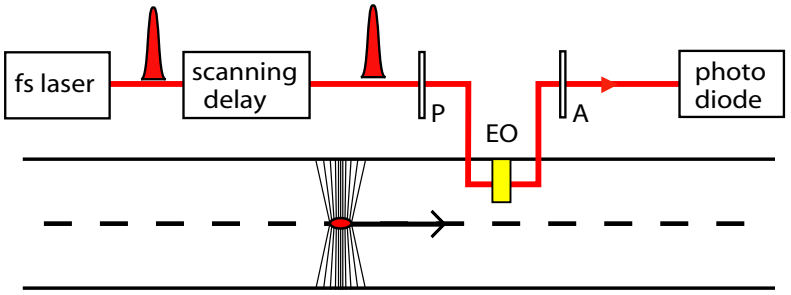

Figure 2.2: Schematic drawing of the setup for electro-optic sampling.

2.2.2 Electro-Optic Spectral Decoding

For spectrally resolved electro-optic detection (EOSD) the longitudinal bunch profile is probed with a chirped laser pulse in a single shot (Fig. 2.3). The chirp is applied by chromatic dispersion. In a dispersive medium group velocity dispersion (GVD) occurs.

The spectral components of a laser pulse propagate through a dispersive medium with different group velocities, resulting in a chirp. For normal dispersion the chirp is negative which means that the wavelength decreases with increasing time [20].

The temporal overlap of the chirped laser pulse and the THz pulse in the EO crystal must be achieved. While co-propagating through the crystal the THz pulse imprints the longitudinal bunch profile on the laser pulse. Due to the chirp a relation between the longitudinal bunch coordinate and the phase retardation of a spectral component of the laser pulse is given. The analyzer section transforms the spectrally dependent phase retardation into a spectral intensity modulation. Once the information is coded spectrally it does not depend on the temporal intensity profile of the laser pulse. That means it can not be disturbed by chirp when propagating through dispersive media like optical fibers. By a spectrally resolving detection the information on the longitudinal bunch profile can be restored.

For EOSD the laser pulses should be chirped with a pulse length T_C which is significantly larger than the electron bunch length.

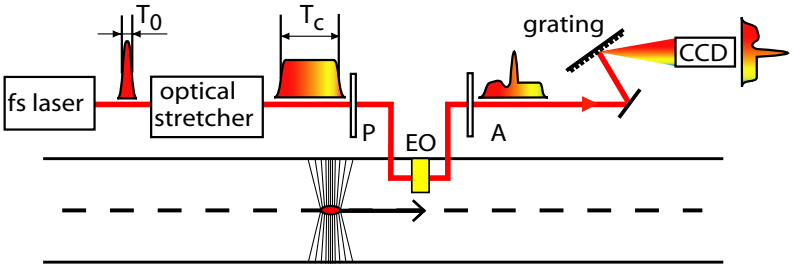

Figure 2.3: Schematic of the electro-optic spectral decoding setup. A spectrometer and a CCD camera are required for the spectrally resolved detection.

2.2.3 Electro-Optic Temporal Decoding

A single-shot technique based on the a temporally resolved electro-optic (EOTD) has first been demonstrated at the Free Electron Laser for Infrared eXperiments (FELIX) [6]. The experimental setup is related to the EOSD setup concerning the modulation of a chirped laser pulse by THz field induced birefringence. Distinct from the spectral intensity modulation investigated in EOSD, the temporal intensity profile of the laser pulse is imaged by single-shot cross-correlation by second-harmonig generation (SHG) in a BBO[1] crystal (Fig. 2.4). Using a EOTD setup a temporal resolution below 60 fs has been reached [8].

The EOTD method requires a complex optical setup close to the beam line and a challenging alignment of an optical cross-correlation. The temporal modulation is not invariant when propagating through dispersive material.

[1] Beta-barium borate

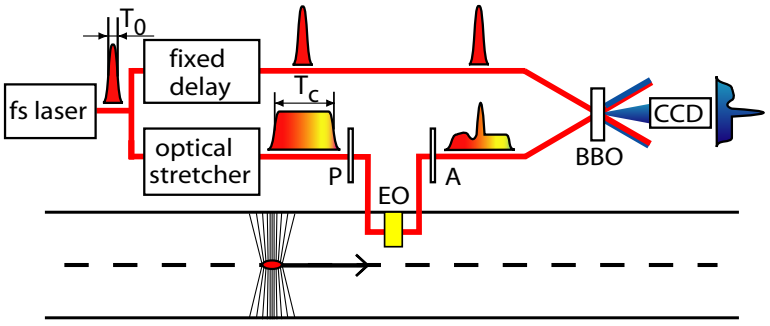

Figure 2.4: Schematic of the temporal decoding setup. The method requires the cross-correlation of a chirped and modulated and a short pulse in a BBO crystal. The light produced contains the information about the longitudinal bunch profile spatially and is detected with a CCD camera.

2.2.4 Spatially Resolved Electro-Optic Detection

The spatially resolved detection method encodes the longitudinal bunch profile in the transverse profile of a single laser shot. In the setup the laser pulse path and the electron bunch path enclose an angle Ψ (Fig. 2.5). The EO crystal surface is perpendicular to the electron bunch path. The crystal is mounted in the plane of the laser path and the electron beam passes the crystal in lower plane. Due to the enclosed angle between the laser pulse path and the crystal surface different spatial components impinge on the crystal at different times. Hence a mapping of time to space is achieved and the longitudinal profile of the Coulomb field of the electron bunch is resolved. The spacial modulation of the laser pulse is detected with a CCD camera.

This method is applied at FLASH to synchronize a laser used for pump-probe experiments to the electron bunch arrival. A time resolution of better than 100 fs has been achieved [21].

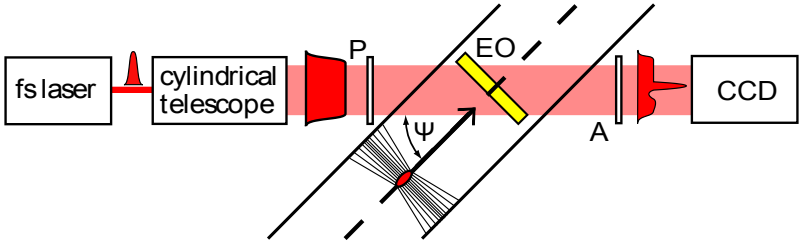

Figure 2.5: Schematic drawing of the spatially resolved detection setup. The electron bunch passes the EO crystal under an angle and in another plane.

3 Experimental Setup

In this chapter, the key components of the experimental setup are introduced and their function is described. The components can be categorized in the laser and its synchronization, the EO front end, the spectrometer and the electronics and opto-electronics used for timing and gating. A schematic overview of the entire setup is shown in figure 3.1. Photographs of the components are shown in the appendices.

This chapter also contains a treatment of the technical requirements for specific components as well as manufacturer specifications. The results of characterization measurements achieved during the commissioning of the components can be found in chapter 4.

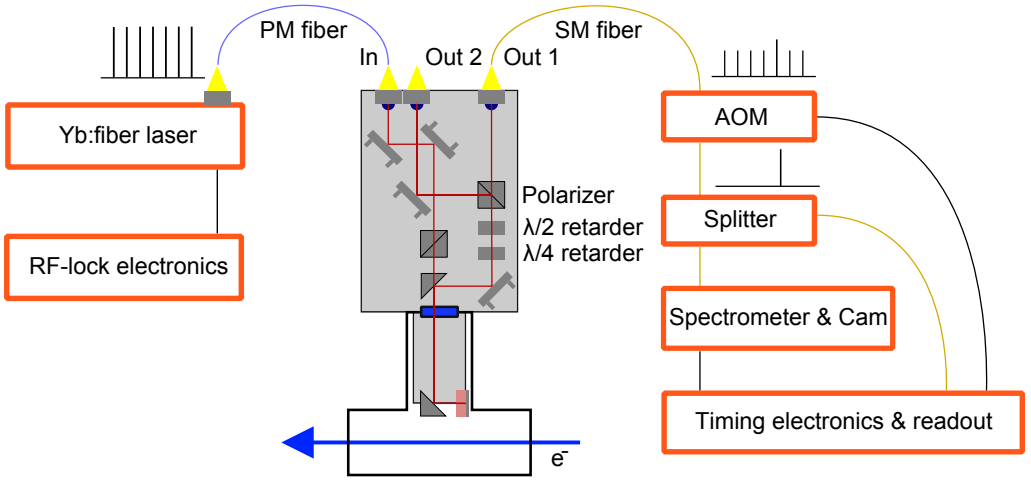

Figure 3.1: Schematic of the EO monitor setup. The EO front end is mounted on the accelerator beam pipe. Components within orange frames are installed inside a lead-shielded electronics rack next to the beam pipe.

3.1 Ytterbium Fiber Laser

The utilized laser system is a commercial ytterbium-doped fiber laser[1] [22]. It is a pulsed laser with a spectral bandwidth of a few ten nanometers as requested for measurements based on EOSD. The central wavelength of 1030 nm provided by a Yb:fiber laser fits the optic properties of gallium phosphide (GaP), the material used for the electro-optic crystal, very good. These are high transmission for the laser light and a good phase matching of the

[1] Orange by Menlo Systems

electric THz pulse and the laser light, which means they have nearly the same propagation velocity in this medium [18].

3.1.1 Layout

The laser system contains a stretched-pulse laser oscillator with self-starting mode-lock from nonlinear polarization evolution. The repetition rate of the laser depends on the total length of the light path inside the oscillator. In order to synchronize the laser to the accelerator driving frequency, the accelerator's RF distribution must provide a RF signal that has the same or a multiple frequency as the laser. The laser is running with a repetition rate of 108 MHz which is the 12th subharmonic of 1.3 GHz, the driving frequency of the accelerating cavities.

To keep the laser synchronized to the RF master clock, the laser repetition rate must be adjustable within narrow bounds. Therefore, there are two elements inside the oscillator that can change its length, i.e. its pulse repetition rate: a piezo fiber stretcher and a motorized delay stage. Both are controlled by the synchronization system described in section 3.2. With the piezo fiber stretcher the length of a piece of fiber is changed mechanically by a piezo element. The fiber stretcher is used for fast and exact adjustments of the repetition rate. With a deviation of about 6 µm per 100 V its dynamic range is relatively small. The motorized delay stage changes the oscillator length by increasing or decreasing the length of the free-space section by moving one collimator, mounted on a linear stage. This provides a coarse adjustment to compensate slow drifts.

The oscillator is followed by a pre-amplifier which is an ytterbium-doped gain fiber pumped by a separate laser diode. The gain fiber in the pre-amplifier has a length of approximately 50 cm and ends at the laser main port, an fiber optics connector[2]. This light is used for the EO monitor. Besides the main port the laser system holds two optical monitor ports of low laser intensity, both coupled out from the oscillator and one RF output. These can be used for synchronization and other diagnostics purposes (Sec. 3.2).

The laser system contains a control unit including electronics for internal diagnostics like mode-lock controls and laser intensity, drivers for the laser pump diodes and a control panel with further diagnostics ports. Furthermore, there is an output DC signal which is proportional to the average optical power at the main port and an input for the pump current control. These can be used for an amplitude feedback, described in section 3.2.4. Via a serial interface all laser settings can be monitored and manipulated remotely.

[2] FC/APC type

3.1.2 Requirements

The requirements concerning the laser pulse repetition rate and the capability of establishing an RF synchronization, needed for an integration in the timing scheme of FLASH, have been discussed. The integrated RMS timing jitter, measured against an RF clock, is a criterion for the quality of a RF synchronization. It should be below 50 fs in the frequency range from 1 kHz to 10 MHz for the free-running oscillator, because a high frequency timing jitter can not be reduced by the RF synchronization. The timing jitter can be seen as the temporal deviation of the laser pulse train to a perfect 108 MHz pulse train.

The pulse energy E_{pulse} is a crucial laser property in EOSD because the principle is imaging the charge distribution of an electron bunch with a single laser pulse and analyzing it spectrally. Besides that, the *near crossed polarizer setup* measurement means a methodically low transmission through the analyzer section (Sec. 2.1.4). The laser system has been delivered with a detailed data-sheet. An abstract of it is shown in table 3.1.

The operation inside an accelerator tunnel brings further requirements, that are partially uncommon for a sensitive optical setup. The environment contaminated with dust, acoustic and electric noise makes an air-tight enclosure of all optical components including the laser necessary. Many heat producing components are packed tightly in an enclosed rack. A simple air cooling is installed but temperature fluctuations and drifts can not be avoided. That is a critical issue considering the thermal expansion of optical components inside the laser oscillator. Furthermore the irradiation with neutron and X-radiation can not be shielded completely by lead, meaning a permanent threat, for example, to the sensitive control electronics. Nevertheless, the restricted accessibility and the needed high up time require a stable operation without maintenance work over weeks and months.

Laser oscillator	
Repetition rate	108.28 ± 1 MHz
Repetition rate tuning	± 200 kHz
Monitor ports	
Connector type	FC/APC-SM
Opt. power	≈ 1 mW
Central wavelength	1030 nm
Spectral bandwidth	> 40 nm
Main port	
Connector type	FC/APC-PM
Opt. power	> 150 mW
Central wavelength	1030 nm
Spectral bandwidth	> 30 nm

Table 3.1: Abstract of the laser specifications indicated by the manufacturer.

3.2 Laser Synchronization

For EO measurements, a stable overlap of electron bunches and laser pulses must be achieved with sub-picosecond precision by synchronization to the local RF master oscillator (MO). The RF synchronization system of FLASH delivers RF signals of multiple frequencies. The 108 MHz and the 1.3 GHz signals are used for the synchronization. The required hardware is assembled in a 19-inch housing.

3.2.1 Fast Feedback Loop

Monitor port one mentioned in section 3.1 is used to establish the laser RF synchronization. A photodiode[3] is connected to it, delivering a pulse train with a fundamental frequency of 108 MHz which is the laser repetition rate (Fig. 3.2). From this signal the 12th harmonic is filtered out by a band-pass filter and mixed with the 1.3 GHz signal from the MO. The difference frequency produced is proportional to the difference of the MO frequency and the laser frequency. This error signal is low-pass filtered and digitized by a fast sampling analog-to-digital converter (ADC). A program running on a digital signal processor (DSP) calculates a regulation signal from the incoming error signal and outputs it to a digital-to-analog converter (DAC). This regulation signal is then amplified by a piezo driver, which is connected to the piezo fiber stretcher inside the laser oscillator. A change of the regulation signal causes a change of length of the stretched fiber which influences the laser repetition rate, i.e. the error signal and so on. A feedback loop is created. With an adapted set of regulation parameters the regulation minimizes the error frequency and locks the laser to the MO.

As it is the fast frequency-adjusting element, the combination of fiber stretcher and regulation operate to an upper regulation threshold of 1 kHz. The dynamic range of a piezo fiber stretcher is finite, so thresholds for the amplitude of the regulation signal must be set. If the regulation signal reaches a threshold, the delay stage is moved, causing a rough change of the laser oscillator length. Nevertheless, the RF synchronization stays established at any time because the fast feedback loop compensates the change caused by the delay stage with the piezo fiber stretcher which is then, assuming a good choice of regulation parameters, set back to the center of its dynamic range.

The ADC, DSP and DAC are VME[4] components in a crate inside the shielded electronics rack. The FLASH network infrastructure enables a remote control of these components.

3.2.2 Phase Detection

As described above, the laser is synchronized to the MO with the 12th harmonic of the repetition rate. Thus, the laser can be locked into twelve different states that can not

[3] EOT 3500 F, 15 V bias voltage
[4] Versa Module Eurocard

be differentiated so far. The slow phase detector[5] is used to resolve this unambiguity. It compares a 108 MHz signal from the MO and a signal from the laser-internal photodiode with the same frequency. A signal with an amplitude that depends on the relative phase of the input signal is produced and read by an ADC. In case of a synchronized laser the relative phase is constant and the slow phase detector outputs a DC signal (Fig. 3.2). The relative phase at which the overlap of the THz pulse and the laser pulse is established determines the operating point of the EO monitor (Sec. 4.3.2).

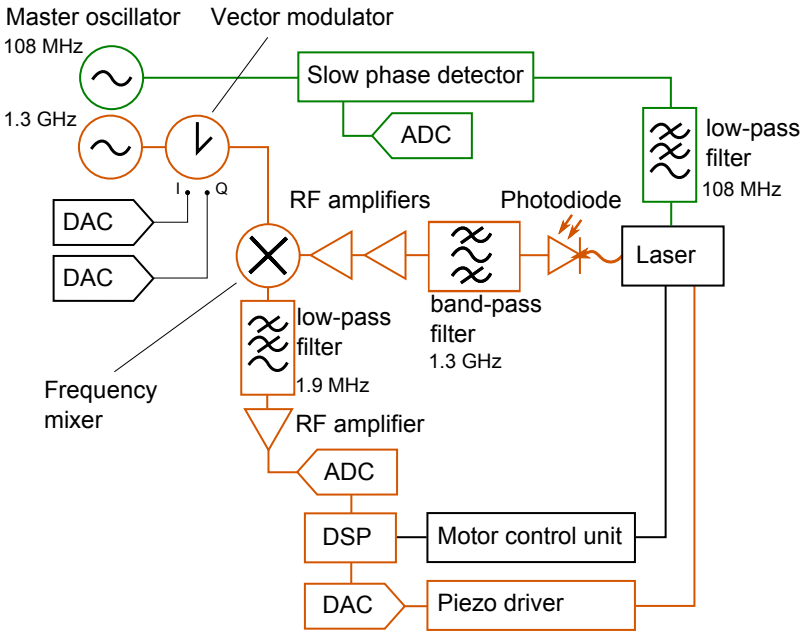

Figure 3.2: Schematic of the RF synchronization of the laser, including the fast feedback loop at 1.3 GHz (orange) and the slow phase detection at 108 MHz (green).

3.2.3 Vector Modulator

A vector modulator (VM) is used to shift the phase of the 1.3 GHz RF signal from the MO before it is delivered to the frequency mixer. Driving the VM means shifting the phase of the signal the RF synchronization locks the laser to. If the step size of those shifts is small enough, the fast feedback loop can follow. The effect is that the arrival-time of laser pulses can be changed relative to the phase of the 1.3 GHz signal and, therefore, relative to the arrival-time of electron bunches in the accelerator.

The VM shifts the phase of an input RF signal by an angle defined by two voltages (I and Q) and outputs the phase-shifted RF signal with an unchanged frequency. I and Q are computed and output via a DAC to the VM in a way that their sin and cosine, respectively, define the angle of phase shift. Driven at 1.3 GHz a full rotation corresponds to 770 ps. In section 4.3.2, the procedure of a *fine timing scan* is described, using the vector modulator to find the temporal overlap between the THz pulse and the laser pulse.

[5] Desy-internal AD8302

3.2.4 Amplitude Feedback

Controlling the optical output power of the laser is needed to achieve a constant laser intensity during EO measurements. The laser system is designed for an amplitude feedback as it provides an optical power output and a modulation input. An amplitude feedback can be established with little effort. Using physically the same ADC, DSP and DAC, another feedback loop in parallel to the RF synchronization is created, as these components can run multiple feedbacks on the same hardware. Distinct from the fast regulation for the RF synchronization, the amplitude feedback compensates drifts of the output power of the laser pump diodes in a range of minutes and hours.

3.3 Electro-Optic Front End

The EO front end holds the electro-optic crystal inside the beam vacuum and is mounted directly on the electron beam pipe. It contains all free-space optics components necessary under a cover to protect them from dust and mechanical destruction as well as securing the environment from the hazardous laser beam. The front end is constructed as compact as possible and requires only about 10 cm of beam pipe to be installed. See figure 3.3 for a technical drawing.

Designed at the Paul-Scherrer-Institute (PSI) in Switzerland, the EO front end features a simple as possible setup with the possibility to remotely control the angle of both retarders in the analyzer section. The design also allows to vary the distance between the electron beam and the EO crystal without changing any free-space optics. To achieve this, the entire monitor can be moved vertically by a motor. A flexible bellow connects the electron beam pipe and the vacuum part of the monitor. The flexibility of the optical fibers compensates the occurring movements in the centimeter range.

A polarization maintaining optical fiber (PM fiber) patch cord with a length of 2 m is necessary to transport the laser light from the pre-amplifier output into the EO front end. In this minimal amount of dispersive medium a part of the chirp needed for EOSD is added. The optical path leads through a polarizer and a vacuum window to a mirror where the laser beam is reflected into counter-beam direction. It enters the GaP crystal which has a thickness of 500 µm in electron beam direction.

To achieve a better transmission, an anti-reflective coating is applied to the crystal surface. The opposite side of the EO crystal carries a high reflective coating. As the electric field of the passing electron bunch is supposed to enter the crystal at the leading edge, the reflective coating can not be a metallic mirror but must be highly pellucid for electro-magnetic fields in the THz range. In case of an temporal overlap the THz pulse and the laser pulse co-propagate in the direction of the electron beam through the crystal.

Having left the crystal, the laser beam is guided back trough the vacuum window and

into the housing of the EO front end. The optical beam axis inside the front end is tilted in the figure plain, leading the laser beam coming from the EO crystal to a mirror. It enters the analyzer section, consisting of two retarders and a polarizing beam splitter. The optical free-space path ends with two collimators. Only one polarization plain is needed for detection in EOSD. The beam is collimated into an optical single-mode fiber (SM fiber) to transport the light back into the shielded rack.

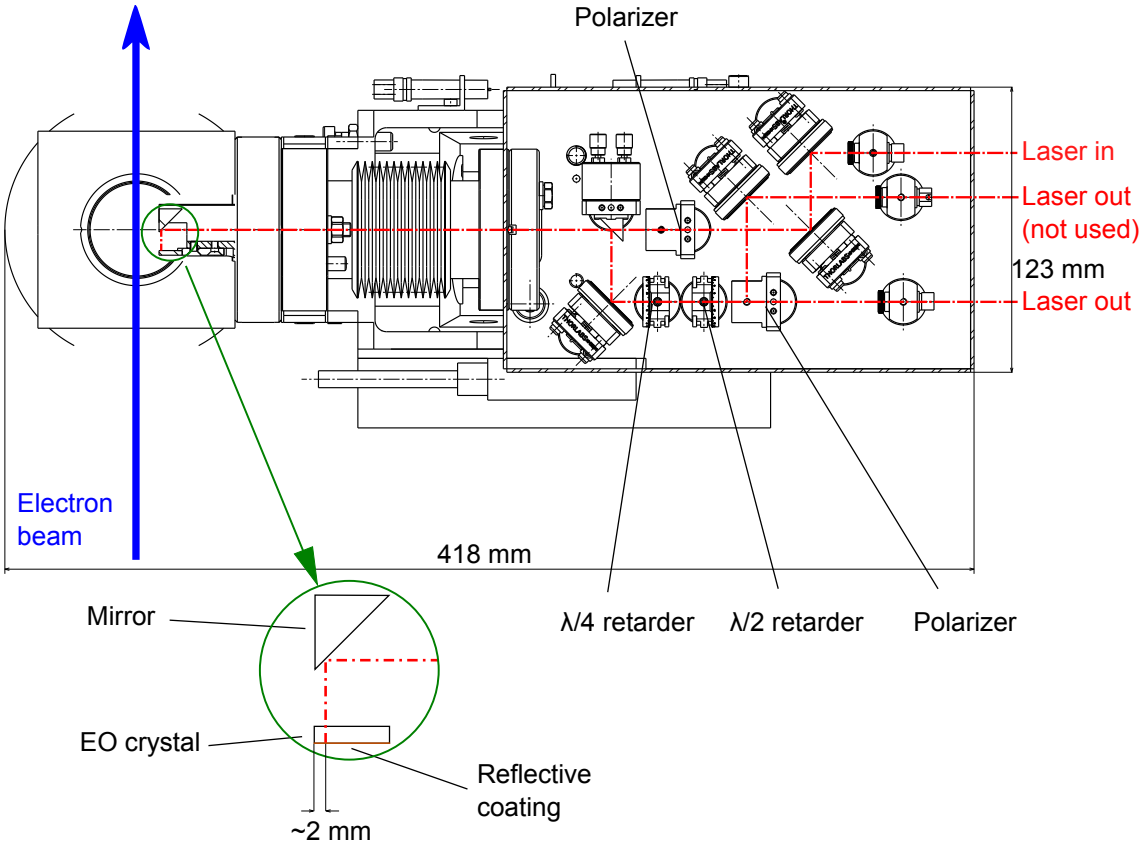

Figure 3.3: Schematic of the EO front end. As opposed to the drawing both retarders are motorized. The crystal thickness of 0.5 mm in beam direction is not drawn to scale.

3.4 Gating

The laser pulse train coming from the EO front end still has the full repetition rate of 108 MHz whereas the repetition rate of FLASH is 10 Hz (Sec. 1.1.4). Assuming a single-bunch operation scheme and a temporal overlap, just one out of $1.08 \cdot 10^7$ laser pulses is modulated by the electro-optic effect. A precise timing and gating is needed to pick the modulated pulse out of the pulse train for further analysis while blocking all other pulses. As the gap between to laser pulses is approx. 9 ns, an optical gate must open for a time of that order of magnitude. The minimal camera exposure time is too long for this demand, so an acousto-optic modulator (AOM) is used as an optical pulse picker for gating the laser

pulse train.

The functional principle of the AOM is as follows: light coming from an optical fiber is entering a crystal. Perpendicular to its direction of travel, acoustic waves are created inside the crystal by a piezo transducer. The result is a periodic density modulation inside the crystal material at which diffraction of the light occurs, producing a deflection. Only in case of a certain deflection, the light is coupled into the outgoing fiber of the AOM, which means the AOM opens if RF power is supplied to the piezo transducer.

For this setup an AOM[6] and driver with a driving frequency of 200 MHz is utilized. The high extinction ratio of the closed AOM is crucial for suppressing unmodulated laser pulses. The extinction ratio of the AOM is specified by manufacturer to be 50 dB. The exposure time of the camera is 70 µs. This yields a signal-to-background ratio of 13.2 due to AOM leakage.

The gating is implemented by triggering the AOM driver with a 10 ns (nearly) rectangular pulse, provided by a pulse generator[7], which opens the AOM for a single laser pulse. The single pulse is directed to the spectrometer unit which enables a single-shot spectrally resolved detection. The rise/fall-time (10 % to 90 %) is specified to be 7 ns.

3.5 Timing

The detection of electron bunches with lengths in the picosecond range requires a precise timing of a number of processes. One of them is about gating the modulated laser pulse with the AOM. This is called the *rough timing set-point* in this thesis. Another issue is the temporal overlap between the electron bunch and the laser pulse, both having lengths in the picosecond range, inside the EO crystal. This targets the order of magnitude of precision that must be achieved with the *fine timing scan*. The application of both methods is described in section 4.3.

3.5.1 Rough Timing Set-Point

Determining the correct timing for the optical gate is done by temporal comparison of one signal from the electron bunch and another signal representing the gated laser pulse (Fig. 3.4).

Outside a vacuum window under the EO front end a pickup antenna has been installed at a distance of a few centimeters to the center of the electron beam pipe. This antenna receives an electro-magnetic field radiated by the passing electron bunch. Amplified by an RF amplifier it is read by a fast sampling ADC. Another ADC channel reads out the amplified signal of the gated laser pulse, converted by a photo diode. A fiber splitter is used behind the AOM to provide the ability for a *rough timing set-point* search as well as

[6] Gooch & Housego Fibre-Q
[7] Stanford DG535 Pulse Generator

for analysis by the spectrometer. The multiple input channels of the ADC have a common sampling time that can be changed with a step size of 1 ns by an external delay.

The signal propagation times in optical fibers and coaxial cables are not negligible for the intended precision of a few nanometers. Thus, they must be calculated using

- the length of the free-spaces traversed by the laser light,
- the single-mode fiber lengths,
- the coaxial cable length used for electric signals,

and the signal propagation velocity in each of these media. An approximation of the propagation times can be seen in figure 3.4 for the gated laser pulse signal (orange) and the pickup antenna signal (green). The delay that occurs in the amplifiers and the following cables cancels, because equal components are used for both paths. A delay of 27 ns for the signal on the photodiode relative to the pickup antenna signal is obtained.

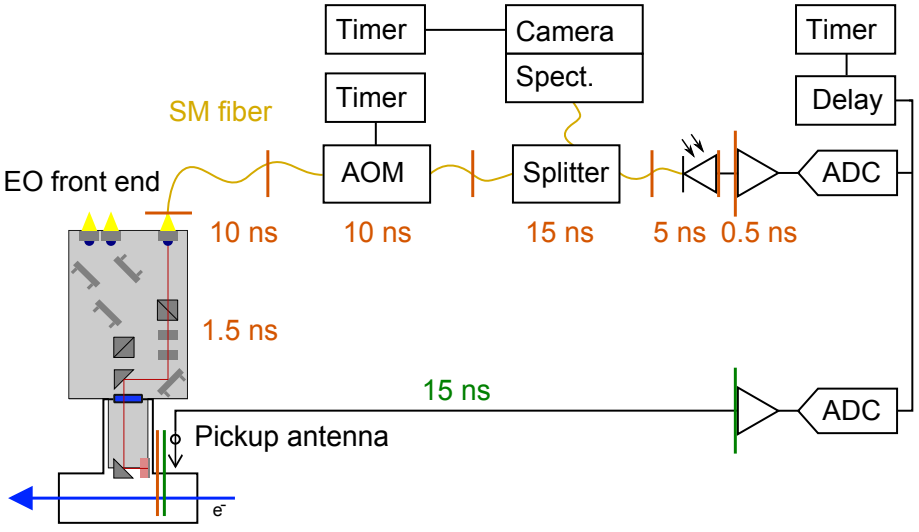

Figure 3.4: Overview of components relevant for the *rough timing set-point*. The propagation times of two signals, the gated laser pulse (orange) and the pickup antenna signal (green), are shown.

Having this information it is possible to trigger the AOM in a way that it provides an open gate for the specific laser pulse that traversed the EO crystal in the moment a passing electron bunch induces a RF signal in the pickup antenna.
Due to technical restrictions the position of the gate can only be shifted with an increment of 4 ns. Remaining propagation time uncertainties result from uncertainties in the measurement of the path lengths and the neglected deviation in propagation time of the laser pulse traveling through optic components like the vacuum window and the polarizing beam cube inside the EO front end and the crystal inside the AOM. The errors are estimated to be of the order of 4 ns.

3.5.2 Fine Timing Scan

The *fine timing scan* is done by a vector modulator scan with a step size of a few picoseconds. Scanning with the VM shifts the laser relative to the MO. As the gate is fix relative to the MO, the laser pulse is moved through the gate. Considering the laser repetition rate of 108 MHz, the initial state is reproduced after a scanned range of approx. 9 ns. The *fine timing scan* requires an analysis of the gated laser pulse because the modulation caused by interaction with the THz field of the electron bunch must be detected. The modulation can be seen in the pulse intensity as well as in its spectral intensity distribution. The first can be analyzed by the photo diode mentioned and by the spectrometer as well whereas the latter can be detected using the spectrometer. A spectrally based detection method is described in section 4.3.2.

3.6 Spectrometer

The spectrograph and the camera are mounted to one spectrometer unit as they are well adapted for each other (Fig. 3.5).

3.6.1 Spectrograph

The spectrograph[8] utilized in this setup is based on a Czerny-Turner optical design with a focal length of 163 mm. The use of a slit is not necessary because the polished end of a single-mode fiber with a core diameter of 9 µm fulfills the requirements of a point-like light source already. An adapter fixes the fiber connector[9] inside the spectrograph in a way that the end of the fiber connector is in the focus of the first focusing mirror, imaging it on a reflective diffraction grating with 600 lines per mm. A second cylindrically focusing mirror images the spectrum on the CCD array of the camera.

3.6.2 Camera

A line scan CCD camera[10] with a 512 channel detector is used. Each channel has a width of 25 µm and a height of 500 µm. The quantum efficiency of the InGaAs detector is about 80% for a wavelength of 1030 nm and the camera sensitivity is specified to be 90 electrons per camera count. It is used with an exposure time of 70 µs. For EOSD measurements in the *near crossed polarizer setup*, the intensity of the laser beam in the spectrometer is expected to be only a few per mill of the intensity at the laser main port. For a successful operation, the camera must be sensitive enough to resolve the optical spectrum of a single laser pulse with a satisfactory signal-to-noise ratio.

[8] Andor Shamrock SR-163
[9] FC/APC type
[10] Andor iDus DU490A-1.7

The camera is triggered by an external timer and is, therefore, synchronized to the whole setup. To reduce camera noise due to dark currents, the detector can be cooled by a Peltier-element. Its heat is dissipated by an air cooling. If it becomes apparent that the air cooling is not sufficient in the environment of the electronics rack, a water cooling can be applied. Spectrograph and camera fulfill the requirements of compact size and robustness. The internal free-space section is air-tight to protect the optics from dust. This includes the fiber connector mounting as well as the transition from the spectrograph to the camera.

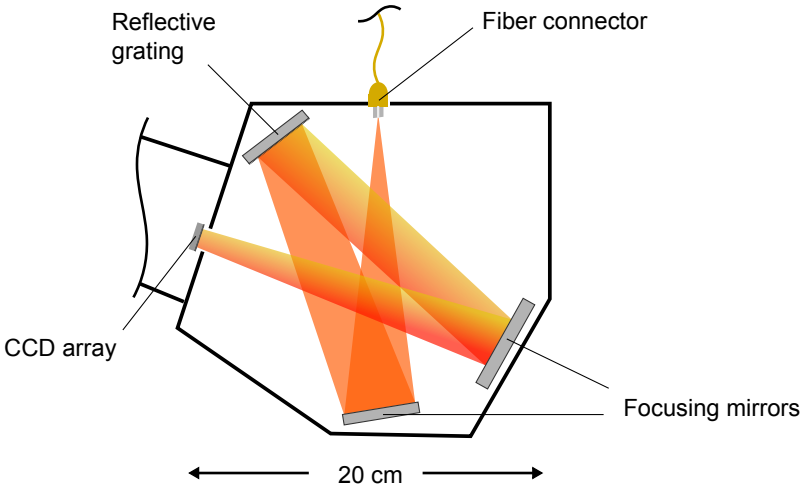

Figure 3.5: Light path inside the spectrograph. The light is inserted directly from a fiber connector. Two focusing mirrors illuminate the diffraction grating and image the laser spectrum on the CCD chip of the camera, respectively.

4 Characterization of Key Components

In this chapter significant results from specification measurements of the key components of the EO monitor system are presented. The first part of commissioning took place in a laser laboratory where measurements for the laser specification have been done. The assembling and commissioning of synchronization electronics and a period of successful stability tests of the laser and the RF synchronization under laboratory conditions followed.

Having obtained satisfying results, the setup has been moved into the accelerator tunnel for further commissioning and long time measurements on the stability and reliability have been performed. As the FLASH tunnel is an restricted area during operation, access is only possible on maintenance days. The combination of maintenance days and machine operation periods offered advantages in developing a method for determining the *rough timing set-point*. The *fine timing scan*, the method the temporal overlap has been established with, is described in this chapter.

4.1 Laser Specification

4.1.1 Optical Power and Pulse Energy

For EOSD as a single-shot detection method the laser pulse energy E_{pulse} is a key issue. Assuming a repetition rate of 108 MHz, E_{pulse} can be calculated from the optical power P_{opt}.

The amplified pulses are measured to have a pulse energy of 1.7 pJ at the main port. Losses occur during the transport via fiber and the optical path trough the free-space section inside the EO front end. A measurement of the optical power inside the beam pipe is not possible. Only the optical powers of the beam entering the vacuum and the beam leaving it can be determined. These are 132 mW and 104 mW, respectively. Considering the symmetric optical path an optical laser power of approx. 120 mW can be assumed in the EO crystal. That corresponds to a pulse energy of 1.1 nJ. See table 4.1 for an overview.

Besides the power at the main port, the optical power at monitor port 1 is of interest as the photo diode for RF synchronization is connected to it (Sec. 3.1). For synchronization purpose, the photodiode must be operated in saturation. Otherwise an amplitude jitter would influence the measurement of the temporal jitter leading to an error in the determination of the laser phase. The result of the power measurement indicates that the monitor port 1 is suitable for the operation in the feedback loop for the RF synchronization in com-

bination with a fast photodiode. The optical power has been measured using a Thorlabs PM 100 A.

	P_{opt} (mW)	E_{pulse}(pJ)
Monitor port 1	2.6	24
Monitor port 2	4.3	40
Main port	11.7	108
Main port (amplified)	183	1690
EO crystal	$\approx$ 120	$\approx$ 1110

Table 4.1: Measured optical power P_{opt} and calculated pulse energy E_{pulse} at the three laser ports and in the EO crystal.

4.1.2 Optical Spectra

As a mode-locked laser starting from nonlinear polarization evolution, the laser has a spectral intensity distribution typical for its design. Nevertheless, the development of an mode-lock state depends on nonlinearities inside the oscillator fiber in combination with other oscillator-internal components. This causes a variety of mode-lock states. The most significant characteristics are their optical spectra, four of them are shown in figure 4.1. The states also differentiate in the commonness of appearance. Figure 4.1d represents a very common mode-lock state while figure 4.1a shows a spectrum that appears very seldom. The mode-lock control is automated to a great extent and it can be controlled remotely. All spectra have been taken with an ADVANTEST Q8384 Optical Spectrum Analyzer.

Besides the spectral intensity distribution, different mode-lock states can differ in the optical output power from the oscillator and in their stability, especially when establishing the RF synchronization. The repetition rate is determined by the length of the oscillator and hence is equal for all mode-lock states. The optical power from the main port is not mode-lock state dependent because it is dominated by the pump diode intensity of the pre-amplifier and not by the optical power it is fed with.

A special behavior of this type of laser is the occurrence of double-pulse states. In such a mode-lock state, two laser pulses circulate inside the oscillator with a fixed distance in time of a few picoseconds. Double-pulses separated only by some picoseconds are difficult to detect as the interval between the two pulses is too small to have a measurable impact on the spectrum due to interference but too large to be covered by the dynamic range of an autocorrelator. Nevertheless, the spectrum shown in figure 4.1c might indicate such a double-pulse state.

The spectrum from the main port of the laser is modified as it passes the gain fiber of the built-in pre-amplifier. The effect inducing the spectral change is called gain narrowing, caused by the smaller optical bandwidth of the gain spectrum of the fiber amplifier. Fig-

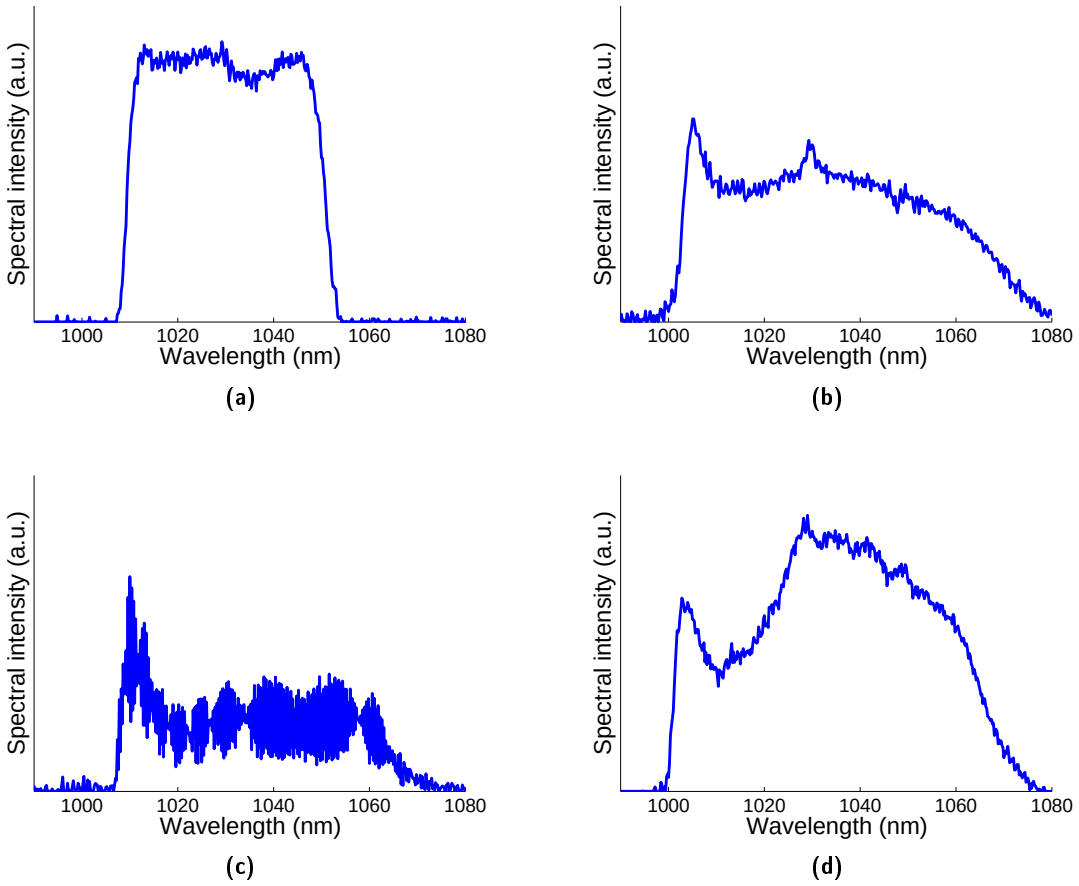

Figure 4.1: Spectra of different mode-lock states, taken from monitor port 1. The spectrum in (d) is typical for the most common mode-lock state.

ure 4.2 shows the spectra from the main port with the amplifier pump diodes activated and deactivated, respectively. The gain narrowing depends on the pump intensity. It occurs at activated and deactivated pre-amplifier as well and a shift of the central wavelength can be observed.

The usable bandwidth for EOSD must be determined experimentally. Usually, it is higher than the measured FWHM bandwidth $\Delta\lambda$ of 37 nm measured at the main port. The central wavelength is determined to be $\lambda = 1037\,\text{nm}$.

4.1.3 Pulse Lengths

The transform-limited pulse length T_0 can be calculated from the spectral bandwidth $\Delta\lambda$ of a laser.

The spectral bandwidth and the pulse length of a laser pulse are connected by the time-bandwidth product [20]. A minimal pulse length can be stated for a given bandwidth and considering the pulse shape and is called the bandwidth-limited pulse length T_0.

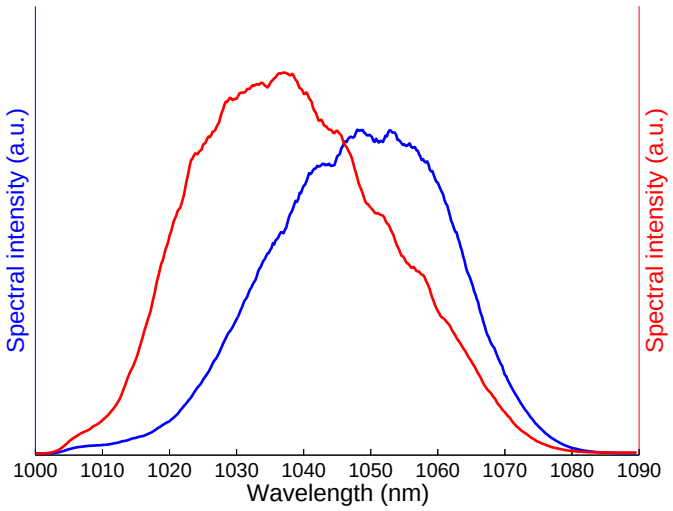

Figure 4.2: Laser spectra from main port with amplifier activated (red) and deactivated (blue).

The dependence of the spectral bandwidth and the minimal pulse length is derived from the Fourier transform which connects these properties. The time-bandwidth product is the determining value, its numeric value depends on the shape of the laser pulses. It reads

$$\sigma_\omega \sigma_\tau \geq c_B \; ; \quad c_B = 1 \text{ for Gaussian pulses.} \tag{4.1}$$

Using the FWHM bandwidth $\Delta\lambda$ and the central wavelength λ stated in the previous section and the relations $T = 2\sqrt{2\ln 2}\;\sigma_\tau$ and $\Delta\omega = 2\sqrt{2\ln 2}\;\sigma_\omega$ for Gaussian pulses, the transform-limited pulse length is

$$T_0 = \frac{\lambda^2}{\Delta\lambda}\frac{2\ln 2}{\pi c} \approx 43\,\text{fs} \; . \tag{4.2}$$

The laser design does not deliver transform-limited pulses to any of the ports, but only chirped pulses from propagation through optical fibers. The determination of the lengths of these pulses can be done with an autocorrelator.

An autocorrelator splits the incoming light into two parts. One part is delayed in an adjustable stage and both rays are combined in a BBO crystal, producing light by sum-frequency generation (SFG). The intensity of the light produced in the crystal versus the amount of delay added to one of the light paths leads to the autocorrelation function (ACF). Considering the shape of the laser pulse, the actual pulse length can be derived from the ACF. For a Gaussian pulse the FWHM of the ACF is larger by a factor of $\sqrt{2}$ than the FWHM pulse length T. Figure 4.3a shows the autocorrelation function of pulses from the main port of the laser. The results of the performed measurements can be found in ta-

ble 4.2. Considering the pulse energy and the utilized fiber lengths, these pulse lengths are dominated by a linear chirp due to group velocity dispersion and will be denoted as T_C [20].

The light transport to the EO monitor requires an additional PM fiber patch cord with a length of 2 m adding linear chirp to the laser pulse. Figure 4.3b shows the autocorrelation function of those pulses. This measurement has been performed with the specific patch cord installed in the setup so the resulting laser pulse length is equal to the pulse length inside the EO crystal. There are only two small sources of chirp in the optical path inside the front end which are the polarizer and the vacuum window which can be neglected. These measurements have been performed using an APE pulse check with a scan time of 150 ps and a photodiode detector. The laser pre-amplifier has been activated.

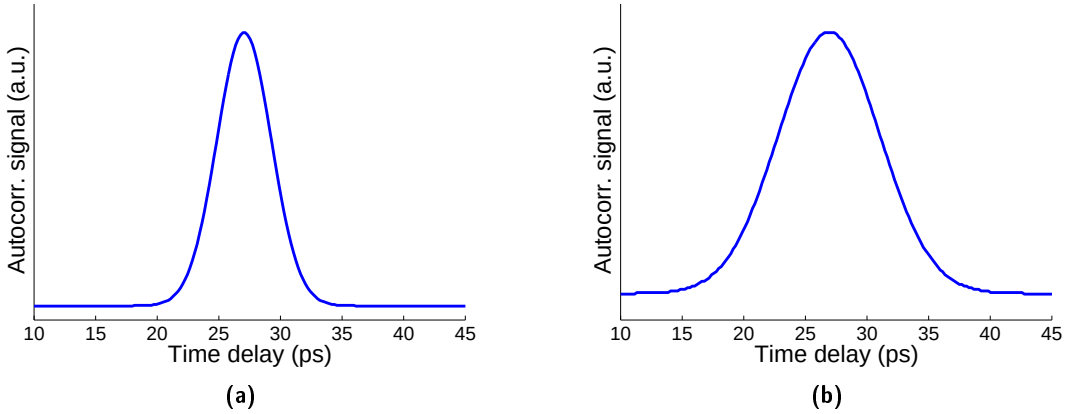

Figure 4.3: Autocorrelation signals of the laser pulse at the laser main port (a) and with additional 2 m of fiber (b).

	ACF (FWHM) (ps)	T_c (FWHM) (ps)
Main port	5.7	4.0
PM fiber, 2 m	10.2	7.2

Table 4.2: Results of the pulse length measurements by autocorrelation.

4.2 RF Synchronization and Amplitude Feedback

The phase noise is an important indicator for the repetition rate stability of free-running lasers, as well as a quality of a RF synchronization. The following measurements have been performed using an Agilent E5052 signal source analyzer (SSA). This device generates a predefined center frequency and compares it to an input RF signal of the same frequency. The result is the single-sideband (SSB) phase noise, giving information about the frequencies of noise the input signal has, allowing a frequency-dependent relation to noise sources.

The following measurements were done out-of-loop using a 10 GHz photodiode[1] connected to the laser main port and a band pass filter. It picks the 1.3 GHz component for analysis with the SSA as this is the frequency the RF synchronization is established with. Besides the SSB phase noise (Fig. 4.4), the integrated RMS timing jitter is calculated from the phase noise data. The integration starts at high offset frequencies. In figure 4.4 there are also the parts of integrated timing jitter given for each logarithmic frequency decade which sum up quadratically.

The ytterbium fiber laser is a mode-locked laser which means it runs autonomous in a pulsed operation state with a repetition frequency given by the oscillator length. Figure 4.4a shows a phase noise measurement of the so called free-running laser. The integrated RMS timing jitter in the frequency range from 1 kHz to 10 MHz is calculated to be 24.6 fs. This high-frequent phase noise can not be reduced by a regulation. The constant noise floor at −150 dBc/Hz is caused by the photodiode restriction. Below 500 Hz the integrated timing jitter increases in several steps until it reaches about 1 ps at the integration limit of 10 Hz. The step-wise increase of the timing jitter is correlated with the sharp spikes in the SSB phase noise, indicating noise sources with the respective frequency. A dominant noise source is the mains frequency of 50 Hz and multiples that are insufficiently shielded by the power supply, driving the photodiode in the out-of-loop setup. An in-coupling of noise from switching power supplies is a conceivable explanation for phase noise in the region of 5 kHz to 9 kHz.

The purpose of the laser RF synchronization by a regulation loop is to make use of the long time stability properties of a RF oscillator. The upper regulation bandwidth cutoff is 1 kHz and the regulation is able to prevent the laser from drifts for many weeks, which makes stating the lower regulation cutoff redundant. Establishing a RF synchronization, the regulation suppresses phase noise in a frequency range up to its cutoff but adds high frequent noise. Figure 4.4b shows an SSB phase noise measurement with the RF lock established, using an adequate set of regulation parameters. The integrated RMS timing jitter in the frequency range from 1 kHz to 10 MHz is increased by the regulation to 56.7 fs which is correlated to a spike at an offset frequency of 10 kHz to 20 kHz in the SSB phase noise plot. The fact that this spike only occurs with an activated regulation points at the components in the regulation loop like the piezo and piezo driver and the digitization progress as possible noise sources. In the frequency range from 10 Hz to 1 kHz, the effect of the mains frequency is still dominant but suppressed by the regulation.

Phase noise measurements require a complex equipment and had been done in a laser laboratory before the laser system has been moved into the accelerator tunnel. The long time stability of the synchronization is determined in a different way called the in-loop measurement.

[1] The same type used for the RF synchronization (Sec. 3.2)

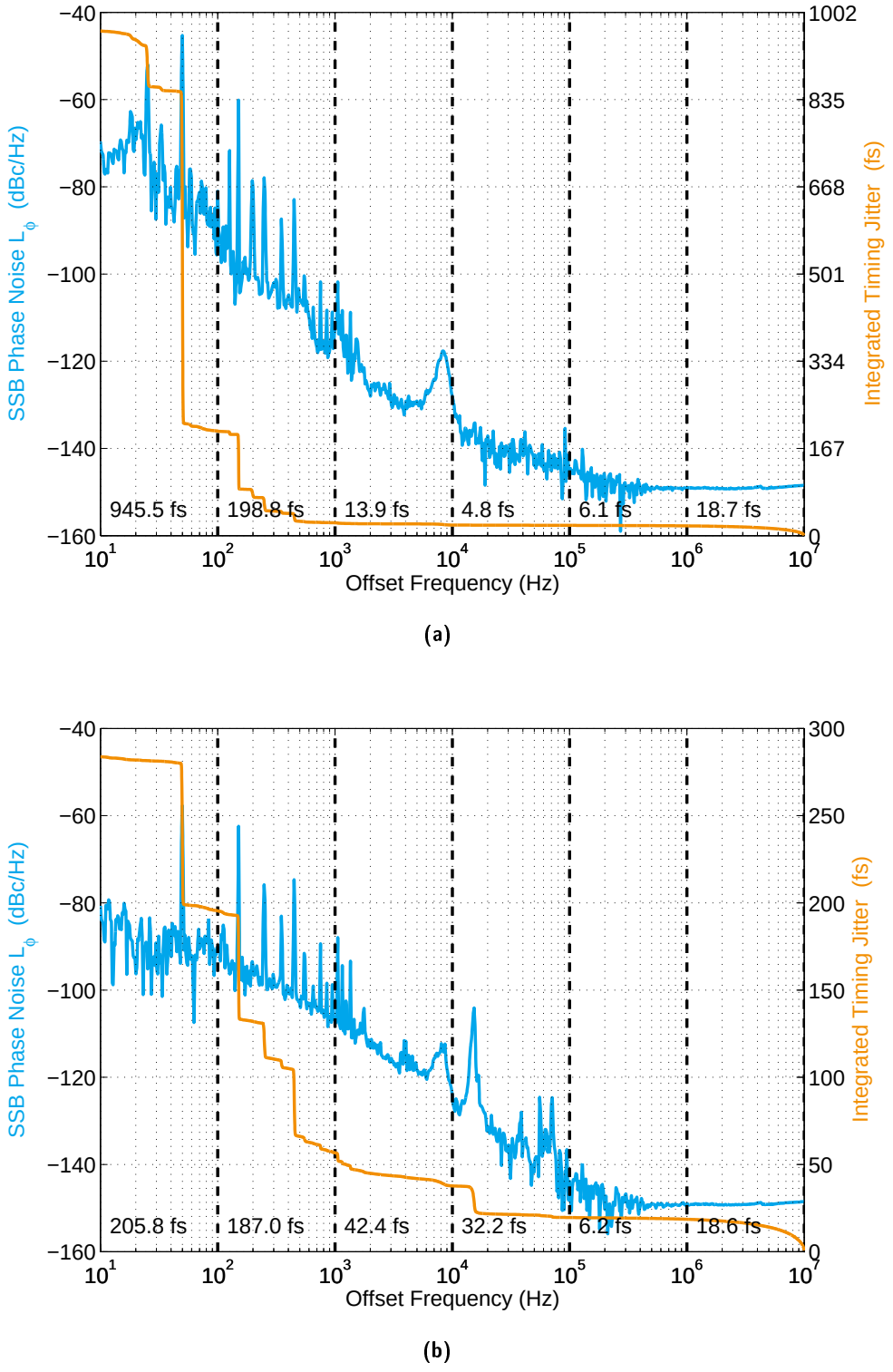

Figure 4.4: The SSB phase noise (cyan) and the integrated timing jitter (orange) of the free-running laser plotted versus the offset frequency is shown (a). Once the RF synchronization is established (b), the phase noise below 1 kHz is decreased, resulting in a lower integrated timing jitter.

In this method the error signal digitized by the ADC (Sec. 3.2) is used to calculate the in-loop timing jitter which, distinct from the out-of-loop method, gives a rough idea of the RF synchronization quality. Nevertheless, the in-loop jitter can be used in an easier way to investigate the long time stability of the laser RF synchronization while the laser is installed in the electronics rack inside the accelerator tunnel.

Using a simple software tool, the read back values for three parameters have been taken every 10 seconds over a period of 108 hours[2]. The plot in figure 4.5 shows the in-loop timing jitter, the piezo fiber stretcher voltage and the delay stage motor position. The most obvious effect of the regulation is the changing piezo voltage for fine adjustments and the delay stage movements for rough adjustments, triggered by the piezo voltage reaching a threshold. The timing jitter exceeding the 55 fs only in a few data points demonstrates the effectiveness of the regulation in keeping a stable, low jitter synchronization of the laser.

The dynamic range of the driver for the piezo fiber stretcher is 10 V to 100 V. Phase noise measurements have shown a strong relation between the piezo voltage and the RMS timing jitter. Piezo voltages below 20 V and above 60 V lead to a severe phase noise, most likely caused by the piezo driver. For this reason the dynamic range had to be narrowed. In figure 4.5 a tendency of increased timing jitter for piezo voltages exceeding 50 V is observable at monitoring hour 30. The narrow piezo range requires more delay stage movements which is, except for mechanical wastage, not a drawback.

If the piezo voltage runs out of bounds, the regulation operates the motorized delay stage automatically, keeping the piezo voltage in its dynamic range. This happened four times during the first 32 hours of the monitoring period. A movement of the delay stage is, depending on the regulation bandwidth, almost instantaneously compensated by the piezo fiber stretcher to keep the synchronization established. Therefore, the step size in the piezo voltage must match linearly a step size of the delay stage. For the motor position plotted in figure 4.5 this does obviously not hold. The reason is a mechanical back lash in the delay stage gearbox. This makes the motor position generally not corresponding to the delay stage position.

During the monitoring period discussed the amplitude feedback has been activated. The read back value proportional to the laser output power which is fed into the regulation loop has been recorded. During 108 hours, the relative RMS standard deviation of the amplitude is 0.18 % and is caused by an amplitude jitter on short time scale. The shot-to-shot amplitude stability is a laser quality and can not be influenced by the regulation. An amplitude drift could not be observed during the monitoring period. This result is based on an amplitude measurement inside the laser system, but does not include any effects on the laser amplitude caused along the optical path to the camera.

[2]The in-loop jitter monitored over a period of a few months can be found in the appendices.

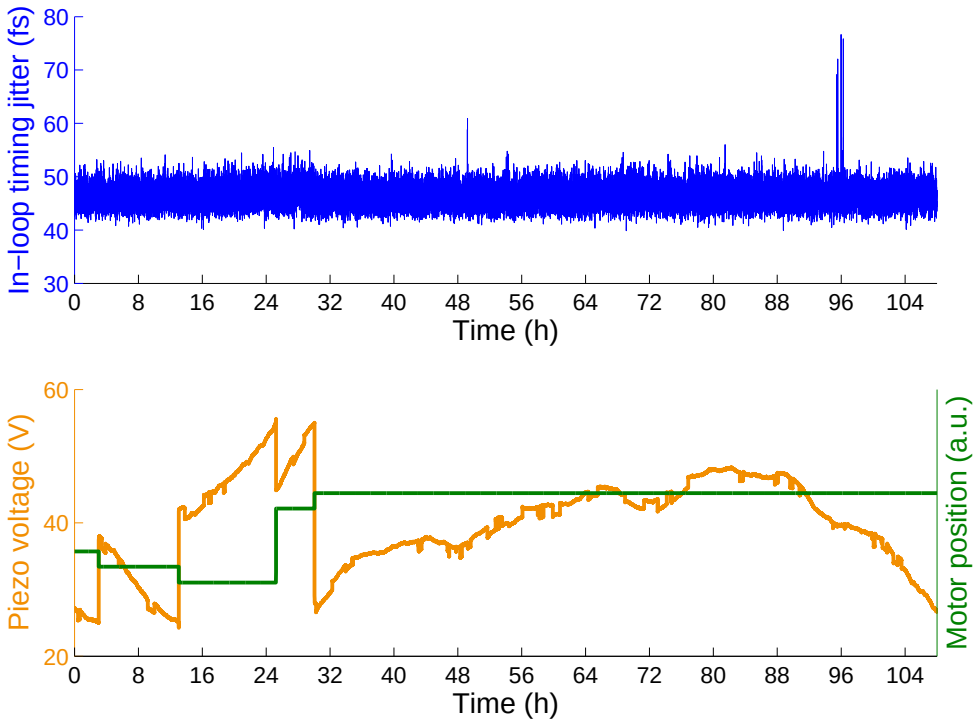

Figure 4.5: Long time monitoring of the laser RF synchronization for a period of 108 hours. The timing jitter has been measured in-loop (blue). The piezo fiber stretcher voltage (orange) and the motor position (green) are controlled by the regulation to keep the RF synchronization established.

4.3 Timing

4.3.1 Rough Timing Set-Point

The *rough timing set-point* defines the opening time of the AOM gate relative to the electron bunch arrival-time at the EO monitor. The time scale for the precision of the set-point as well as the opening time of the gate are in the few nanosecond range. The setup is described in (Sec. 3.5.1).

Scanning the delay of the two ADC channels, the temporal difference between both signal paths can be determined. To get a response from the pickup antenna, sufficiently compressed electron bunches with a typical charge of 0.5 nC have been generated in the accelerator. The region of interest of the pickup antenna signal is the leading slope, as it marks the arrival-time of the electron bunch with a precision of a few nanoseconds. The signal amplitude and width are determined by impedances of the antenna, the coaxial cable and the amplifier and finally by the analog input bandwidth of the ADC. These components are by far not suitable to temporally resolve the Coulomb field of a passing electron bunch. An equivalent argumentation holds true for the photodiode signal which is

not meant to be a measurement of the arrival-time of the laser pulse but an approximation of the temporal position of the gate.

A successful *fine timing scan* has proven, that the *rough timing set-point* is adjusted correctly, if the center of the photodiode signal is measured to be delayed by 35 ns to the very beginning of the ascending slope of the pickup antenna signal (Fig. 4.6). The propagation time delay of the two signals of 27 ns (Sec. 3.5.1) and the half of the FWHM gate width of approx. 6 ns add up to 33 ns. Furthermore, the gate positioning increment has to be considered, leading to the stated *rough timing set-point*. The precision of this method is estimated to be 4 ns.

Having the *rough timing set-point* set, it can not be expected that a temporal overlap between the electron bunch and the gated laser pulse is already established. Only a successful *fine timing scan* can state, whether the gate is set correctly.

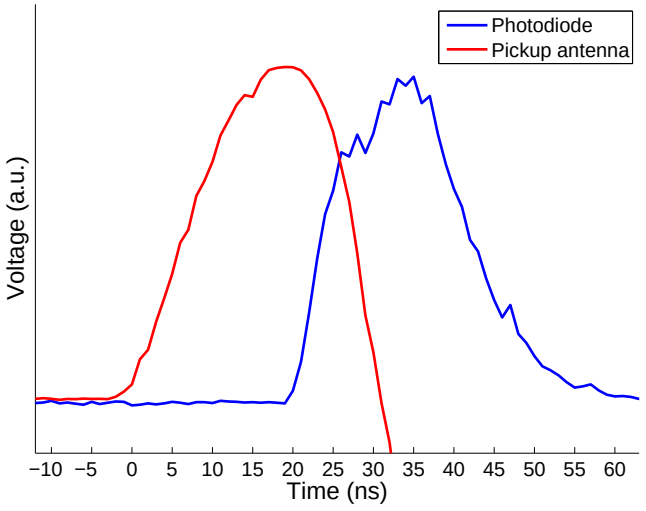

Figure 4.6: The correct *rough timing set-point*. Considering the propagation time difference and the gate width, the center of the optical gate (blue) overlaps the leading edge of the pickup antenna signal (red), which marks the arrival-time of the electron bunch(red).

4.3.2 Fine Timing Scan

The purpose of the *fine timing scan* is to find the overlap of the electron bunch and the laser pulse inside the EO crystal by a vector modulator scan. Due to an optical splitter, laser pulses can be investigated with the photodiode and the camera simultaneously. The *rough timing scan* as well as the *fine timing scan* can be done without changing the setup.

In case of an overlap, the laser spectrum is expected to be modulated in amplitude with a wavelength dependency. During a *fine timing scan*, the spectrometer is used to detect such a spectral modulation caused by the electro-optic effect. For data evaluation, a software

tool has been developed, which compares the spectra taken during the scan with a reference spectrum. To cancel out any wavelength independent amplitude jitter, these spectra are normalized with their total amplitude. The standard deviations for every wavelength division (i.e. camera channel) of the current spectrum and the reference spectrum are taken. The sum over those standard deviations (one for every camera channel), Δ_S is a measure for an amplitude-independent spectral modulation and is plotted versus the time step count of the vector modulator.

In figure 4.7 the result of a *fine timing scan* over a range of 3 ns is shown. The scan has been done in 1 ps steps. For every time step, 10 spectra have been taken and the Δ_S has been calculated (blue dots). Their average is plotted with a red line. Having scanned for about 1.7 ns the overlap has been established. The read back values from the vector modulator (orange) and the slow phase detector (green) determine the *fine timing set-point*. In case of an overlap loss, caused for example by an operating error of the vector modulator, the *fine timing set-point* can be reestablished without the need of performing another scan. However, a constant phase relation of the RF signals provided by the master oscillator (MO) is a pre-condition.

The repetition rate of the laser is 108 MHz which means the time between two laser pulses is approx. 9 ns. Therefore, a scan for 9 ns regardless of the scanning direction brings the system back to its initial state. If there was no overlap found within 9 ns, the gate has been set incorrectly and the *rough timing set-point* would have to be changed before doing another *fine timing scan*.

4.4 Gating and Amplitude Jitter

For the targeted single-pulse gating the opening time of the AOM must be in the same order as its rise/fall-time (Sec. 3.4). Driving the AOM so close to the specified limits has negative effects on the gating performance. The transmission ratio through the AOM is about 60 % for single-pulse gating while 90 % can be achieved if the AOM is fully opened. This has to be considered for the signal-to-background ratio. The problem of higher severity is the shape of the gate opened by the AOM. For illustration purpose gated laser pulses have been measured with a photodiode connected to an oscilloscope operated in persistent-mode (Fig. 4.8). To obtain the shape of the gate, the RF synchronization of the laser has been opened, leading to a statistical distribution of laser pulses in the gate and, therefore, imaging its envelope. The shape envelope is dominated by the bandwidth of the AOM. If the laser is synchronized, the relative position of the laser in the gate is fixed but can be varied by the vector modulator.

The timer signal used to trigger the AOM has a timing jitter of approx. 1 ns relative to the MO whereas the synchronization of the laser pulse to the MO is better by four orders of magnitude. The arrival-time of the electron bunch determines the timing of the laser pulse while an overlap is established. If the gated laser pulse is positioned at a slope of the

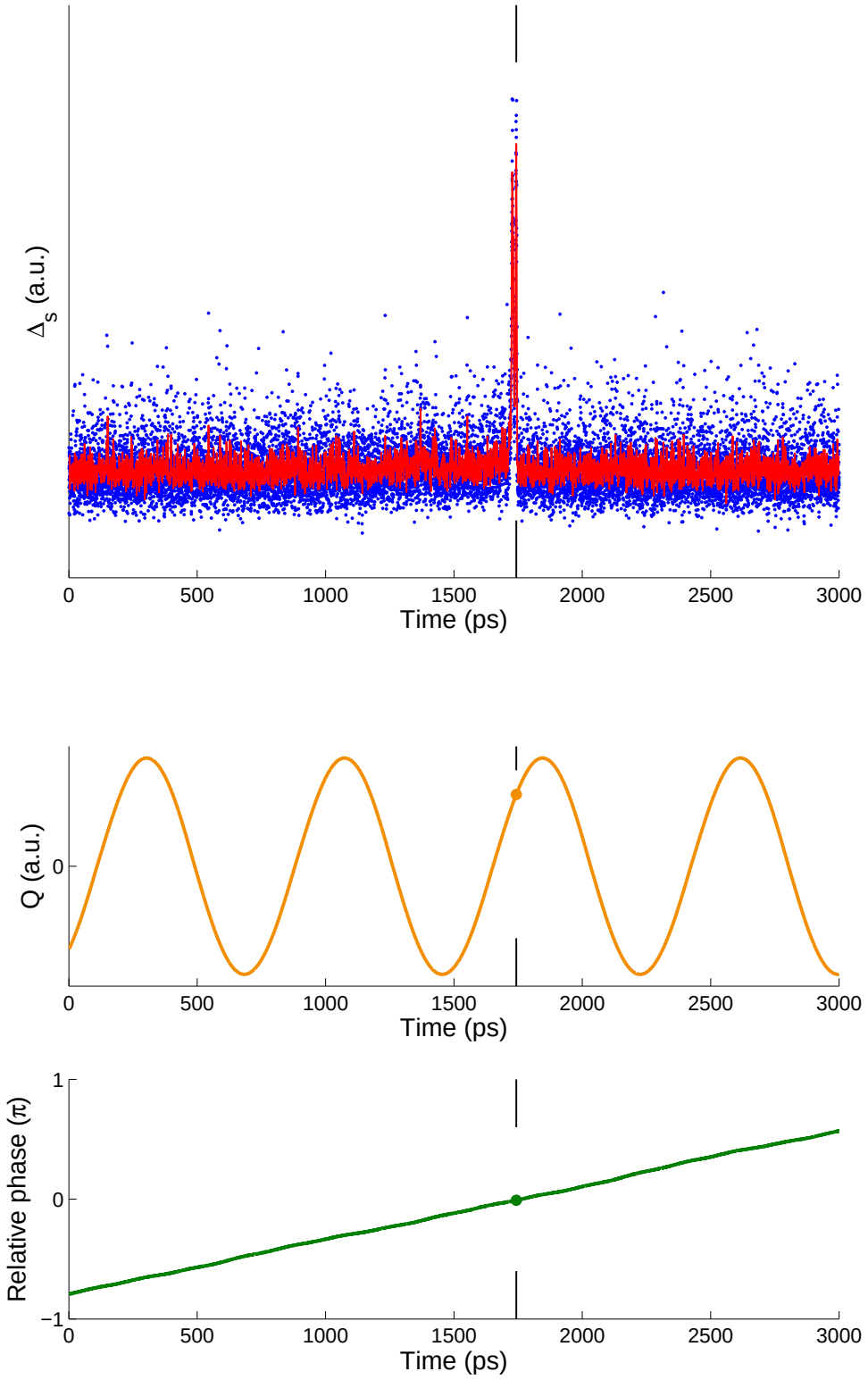

Figure 4.7: First EO signal found with this setup. The average of Δ_S (red) indicates an significant increase of spectral modulation. The vector modulator (orange) and the slow phase detector (green) read back values during the *fine timing scan* are plotted below.

gate envelope, the timing jitter of the gate is transformed into a shot-to-shot amplitude jitter of the laser pulse. The maximum of transmission as well as the minimum of timing jitter to amplitude jitter conversion is achieved at the maximum of the envelope. The gate positioning increment prohibits a fine adjustment of the gate and, therefore, the laser pulse can, in general, not be gated at the ideal point.

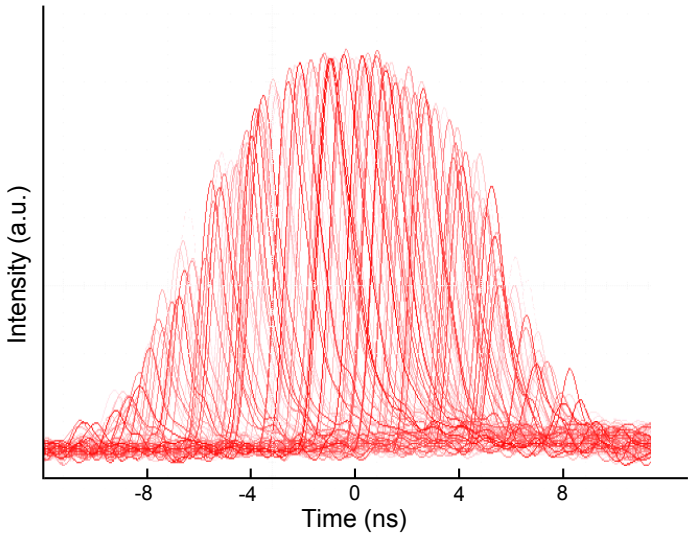

Figure 4.8: Persistent-mode image of laser pulses gated by the AOM, showing the temporal shape of the gate.

5 Data Evaluation

As described in section 1.2 the electro-optic process encodes the temporal profile of the electric field of an electron bunch into the spectrum of the probing laser pulse. The spectrum of the individual pulses is recorded using a commercial grating spectrometer equipped with an InGaAs line detector. To reconstruct the temporal profile from the detector data, a variety of calculations have to be performed. This is done by MATLAB scrips and requires a fraction of the time between two bunch trains which is 0.1 s (Sec. 1.1.4). It provides the capability of quasi-realtime single-shot EO measurements of one bunch in the bunch train at the full repetition rate of 10 Hz.

5.1 Camera Background

Even if no light falls on a CCD camera, it records a signal called dark signal. The sources for a dark signal are dark currents inside the sensor and black body emissions from the surroundings along the optical path. To keep the dark currents as low as possible, the CCD sensor is cooled by an Peltier-element to $-15\,^{\circ}\mathrm{C}$.

For every set of EO measurements, a camera background has to be taken. Therefore, the camera trigger is shifted by several microseconds to make sure that the gate does not open during the camera exposure time. Then, a defined number of camera spectra is taken and averaged. Figure 5.1a shows a typical camera background, averaged from 30 single-shots.

The camera background is dominated by the AOM leakage. It depends on the extinction ratio of the AOM, the camera exposure time and the current retarder settings in the analyzer section. Especially the latter two must be left unchanged for the camera background, the reference spectrum and all further spectra during the EO measurements to have constant conditions. Multiple camera shots are averaged to a camera background to reduce the effect of amplitude jitter. The camera background is subtracted from every spectrum before further data processing.

5.2 Reference Spectrum

To take an unmodulated reference spectrum the gate is shifted by several nanoseconds to earlier times for gating a laser pulse that did not interact with the electric field of a passing electron bunch inside the EO crystal. Taking multiple reference spectra and averaging is

advisable especially to keep the effect of amplitude jitter as low as possible. In figure 5.1b an example of a reference spectrum can be found.

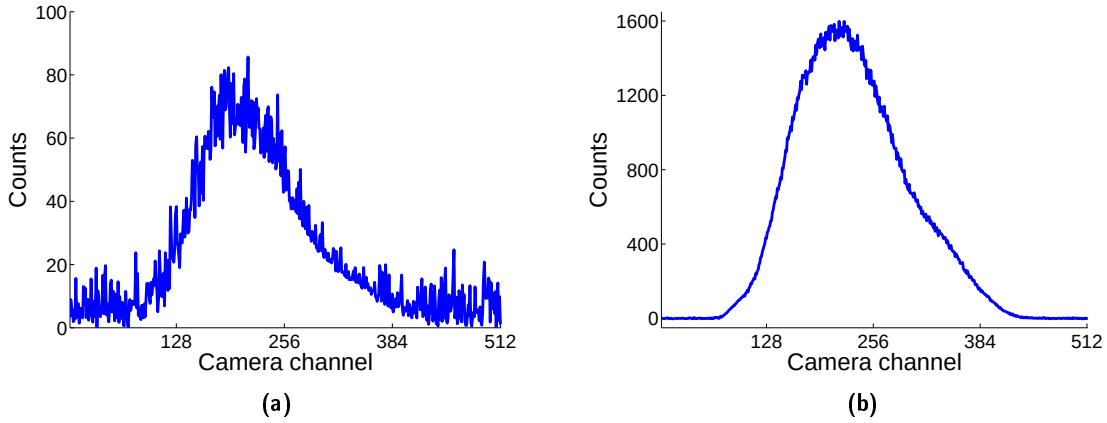

Figure 5.1: Camera background (a) and background subtracted reference spectrum (b), both taken with 30 averages. The retarder settings are $\Theta = 9\,^\circ$ and $\Phi = 0\,^\circ$. The camera exposure time is 70 µs.

The reference spectrum has to be taken for a retarder setting defined by Θ_{ref} and Φ_{ref} in the analyzer section and in the absence of induced birefringence in the EO crystal. Using equation 2.6, the laser intensity I_{las} for every camera channel can be calculated from the reference spectrum, providing an I_{ref} for every camera channel.

$$I_{\mathrm{ref}} = I_{\mathrm{det}}(\Theta = \Theta_{\mathrm{ref}}, \Phi = \Phi_{\mathrm{ref}}, \Gamma = 0) \tag{5.1}$$

5.3 Phase Retardation

The EO signal is evaluated using equation 2.7 and I_{las}, providing a phase retardation Γ for every camera channel. Figure 5.2 shows an example of the evaluation process. The reference spectrum has been taken with 30 averages, 10 averages have been used for the modulated spectrum. The interval on the abscissa is chosen to fit the range that yields useful values for the calculated phase retardation Γ. Regions with counts close to zero for I_{sig} and I_{las} lead to very large fluctuations and can not be used in the analysis.

For EO measurements, the region of interest for Γ reaches from the 140th to the 320th channel. This limits the spectral bandwidth usable for EOSD to $\Delta\lambda_{\mathrm{EO}} \approx 45\,\mathrm{nm}$ which is more than the FWHM of the measured spectral bandwidth stated in section 4.1.2.

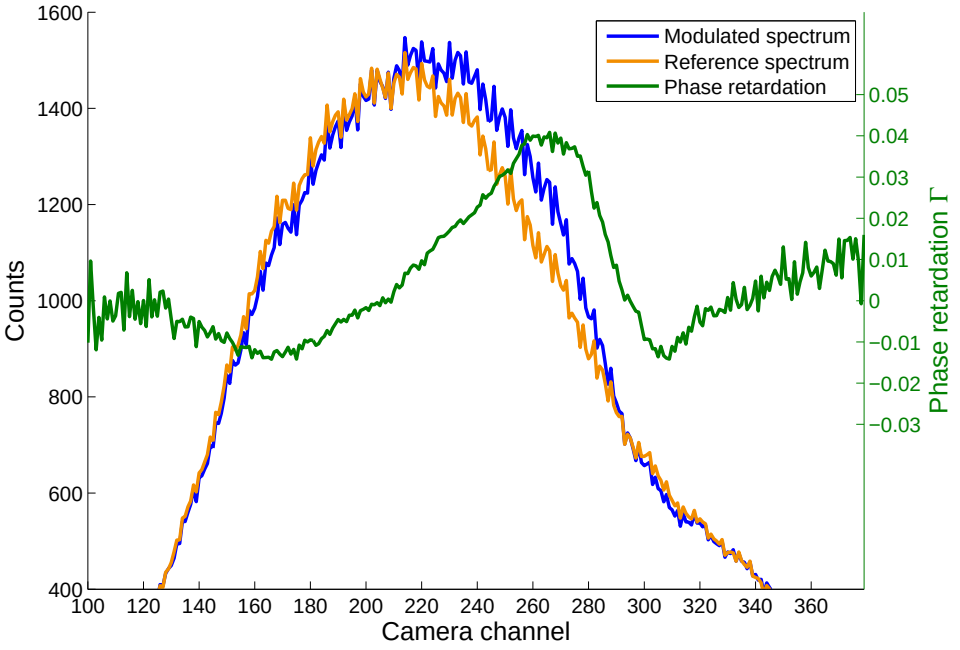

Figure 5.2: Example of the EO signal processing. The reference spectrum is shown in (orange) and the modulated spectrum in (blue). The phase retardation Γ (green) has been calculated according to equation 2.7.

5.4 Time Calibration

For decoding the temporal information from the spectrum represented in camera channels, a time calibration is necessary. The simplest method is the time calibration using the vector modulator (VM). Driving the VM in small steps changes the relative arrival time of the laser beam with respect to the electron bunch. With each step, the overlap is established at a different longitudinal coordinate of the laser pulse and, therefore, at a different wavelength interval. The EO signal is shifted through the region of interest on the camera.

The identification of the EO signal is done by Gaussian fits, shown for every 10th step in figure 5.3a. The centers of the Gaussian functions are evaluated and plotted versus the VM steps of 100 fs for the calibration measurement shown in figure 5.3b. The vertical error bars mark the standard deviations due to the Gaussian fits which are in the order of 0.5 channels. The errors concerning the time axis are caused by the VM, acting as the reference. It has a finite precision, limited by the digitization of the I and Q parameters, which is estimated to be 60 fs. This leads to an error of the data points and is marked in the plot in figure 5.3b. A linear fit yields the time calibration constant of -28.09 ± 0.16 channels per 1 ps. The sign indicates, that the leading edge of a signal corresponds to a higher channel index. The time calibration constant yields approx. 6.4 ps for the range

usable for EO measurements.

To determine an arrival-time from the EO signal, a suitable fit algorithm is required. The method mentioned in this chapter is just one possibility. Fits to the median of the signal as well as fitting algorithms sensitive to the leading edge have been compared without any significant changes on the calibration constant.

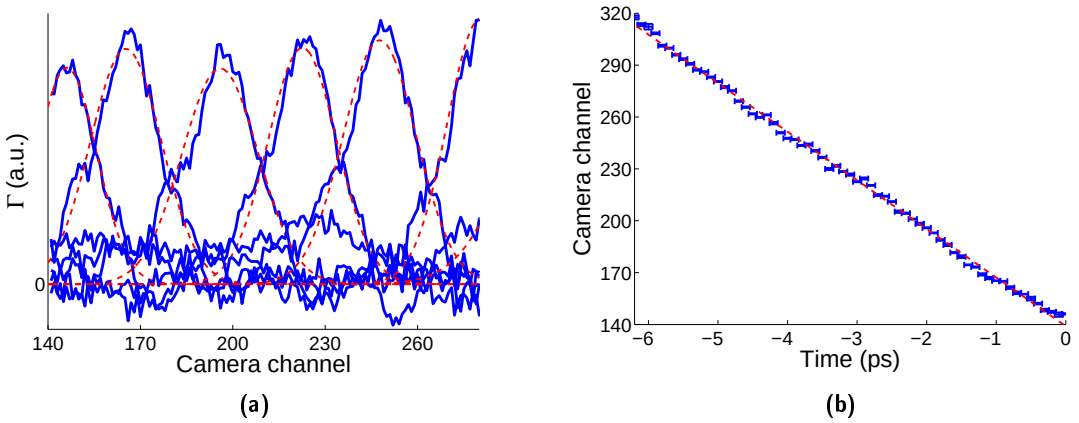

Figure 5.3: EO signal taken every picosecond (blue) and Gaussian fits (red, dashed)(a). Centers of fitted Gaussian fits versus time steps of the vector modulator (blue)(b). The slope of the linear fit (red, dashed) is the time calibration constant.

5.5 EO Single-Shot Measurements

The result of the evaluation process for a single-shot EO measurement can be displayed in a plot of the dimensionless phase retardation Γ versus time. Figure 5.4 shows a sequence of five single-shots EO signals taken in a row. An varying offset can be observed which is caused by amplitude jitter (Sec. 4.4), effecting all spectral components of the laser in equal measure. The calculation of Γ does not distinguish between a spectral intensity modulation caused by phase retardation and a change of the total intensity.

In order to keep the errors due to the offset small, multiple measurements and averaging can be applied. Due to the amplitude jitter the standard deviation of the average Γ is $2 \cdot 10^{-3}$ to $5 \cdot 10^{-3}$ for 10 averages at a constant time. If an EO signal contains the noise-floor (the first 1.5 ps in the signals in figure 5.4), the offset caused by amplitude jitter can be subtracted. The remaining standard deviation after offset subtraction of the averaged Γ is of the order of 1%. In general EO signals do not contain the noise-floor and the amplitude jitter remains as an uncertainty on Γ.

If amplitude fluctuations cause the reference spectrum to be taken with a significant intensity deviation, an offset is caused that is not decreased by signal averages during the following EO measurement. This effect is exceptionally strong in figure 6.6b.

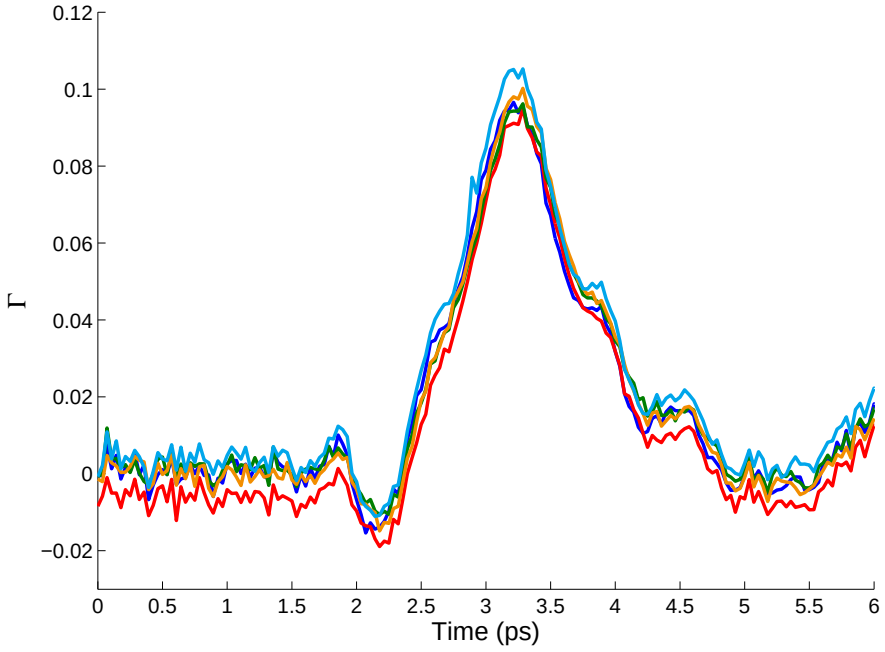

Figure 5.4: Five EO signals taken in single-shot mode successively, shown as phase retardation versus arrival time.

5.6 Signal Merge Method

For some of the measurements presented in this chapter, a time interval longer than the usable range of approx. 6 ps is of interest. Therefore, a method has been be applied where the laser beam is temporally shifted relative to the electron bunch with the vector modulator. Every time step an EO signal is taken. When concatenating these short traces of EO signals, a floating average is calculated to achieve one EO signal trace, covering some tens to several hundreds of picoseconds. See figure 6.1 for an example of a merged EO signal.

A precise relation between the time step of the vector modulator and the temporal information, coded inside the spectrum, has to be considered. Using the time calibration from section 5.4, the EO signals can be merged correctly to a common time axis. All merged EO signals shown in this thesis are calculated with 1 ps time steps, 5 ps time intervals and 10 averages per EO trace.

6 Measurements

In this chapter, results of first systematic studies on the EO monitor system are shown. A part of the following measurements has been done operating the EO monitor in parasitic mode during studies on the accelerator or while FLASH delivered beam time to user experiments. It has been proven, that the monitor can be operated without measurable influence on the SASE process. Furthermore, dedicated accelerator beam time had been requested and granted, offering the opportunity to change machine parameters complying the special needs of the monitor commissioning. Comparative studies have been done with different diagnostics at FLASH as well as with simulation data on the EO process. These data open different possibilities for further characterization of the monitor.

All EO measurements in this chapter have been done in the *near crossed polarizer setup* (Sec. 2.1.3). The best signal-to-noise ratio has been achieved for a set of $\Theta = 9\,^\circ$ and $\Phi = 0\,^\circ$ in the analyzer section.

6.1 Extended Range EO Measurement

Figure 6.1 shows the result of an extended time range measurement of the electric field using the merging method explained in 5.6. The most characteristic features will be discussed here.

At approx. 125 ps the peak in the EO signal marks the arrival-time of the Coulomb field of the electron bunch. A second peak can be observed about 12 ps later and is, most likely, caused by a reflection of the THz field inside the EO crystal. Instead of a co-propagation in electron beam direction (Sec. 3.3), the overlap of the electric field of the laser E_{las} and THz field E_{THz} is established after the latter is reflected at the rear edge of the EO crystal. Both electric fields co-propagate in counter beam direction, are reflected at the front edge of the crystal and co-propagate back. The time delay of the laser pulse required to establish an overlap in that way is 12 ps in respect to the non-reflected overlap.

The surfaces of the EO crystal are coated for transmission and reflection of frequencies of E_{las}, respectively (described in section 3.3), whereas the reflection of an electro-magnetic field in the THz range is about 0.5. For the amplitude of the EO signal caused by reflection one has to consider these losses of the THz pulse intensity as well as the double co-propagation length and the fact, that a Γ caused by the leading pike might add to the

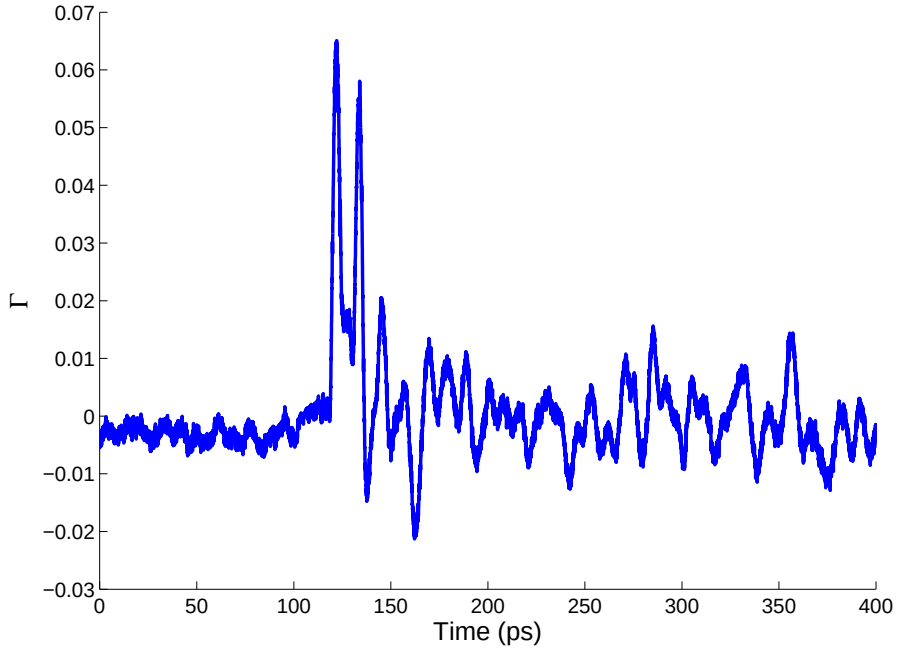

Figure 6.1: Extended time range EO measurement. The first peak at 125 ps is followed by a second peak, caused by reflection. Oscillations due to wake fields that are trailing the electron bunch can be seen.

reflection. For most measurements, the time delay of the reflection is sufficiently high to not influence the EO signal induced by the non-reflected THz pulse. If the EO signal is not taken with the spectrum merge method, the reflection can not be observed, anyway.

The first 100 ps of the EO trace can be used to define the noise floor. The oscillations that are observable from 200 ps on are significantly higher in amplitude and are caused by wake fields trailing the electron bunch. Wake fields are electro-magnetic waves traveling through the electron beam pipe, which are excited by the electron bunch. Their electric field is also detected by the EO monitor leading to irregular oscillations that have been observed for hundreds of picoseconds. At short times behind the electron bunch they are preventing the higher orders of THz pulse reflection in the EO crystal from being observed.

6.2 Radial Dependence of the EO Signal

The EO monitor is based on a measurement of the Coulomb field of the electrons in the bunch described in section 2.1. For $\gamma \approx 300$ at maximum acceleration behind ACC1 the electrons can be assumed to be high relativistic. The electric field is inversely proportional to the radial distance (Sec. 2.1.1). Furthermore, the Gaussian radial charge distribution which is expected for electron bunches is not considered but a sharp-edged distribution is

assumed instead. This approximation can be applied because at the typical distance of the EO crystal to the Gaussian radial charge distribution the deviation can be neglected. Using the relations 2.4 and 2.6 for the *near crossed polarizer setup*, we obtain

$$\frac{1}{\Gamma} \propto r \ . \tag{6.1}$$

This relation can be used to determine the distance from the laser beam in the crystal to the electron bunch via extrapolation.

The radial distance to the beam has been varied by moving the EO front end (including the EO crystal) vertically. EO signals have been taken and the maximum of Γ has been determined (Fig. 6.2). The abscissa in the plot represents the vertical axis of the front end, while zero is the upper limit used as the parking position. A minimal position of about $-27\,\mathrm{mm}$ could be achieved before a direct interaction of parts of the electron beam and the EO crystal occurred. The interaction causes a (partial) beam loss and can be detected with beam loss monitors. This interaction must be avoided to prevent damage to the crystal and to assure the capability of parasitic measurements. Assuming the design values of the chamber and the crystal holder, the center of the beam pipe should be at $-31.6\,\mathrm{mm}$ (Fig. 6.2). The measured beam position from the beam position monitor (BPM) reference to that. The linear extrapolation of Γ traverses the abscissa at approx. $-35\,\mathrm{mm}$.

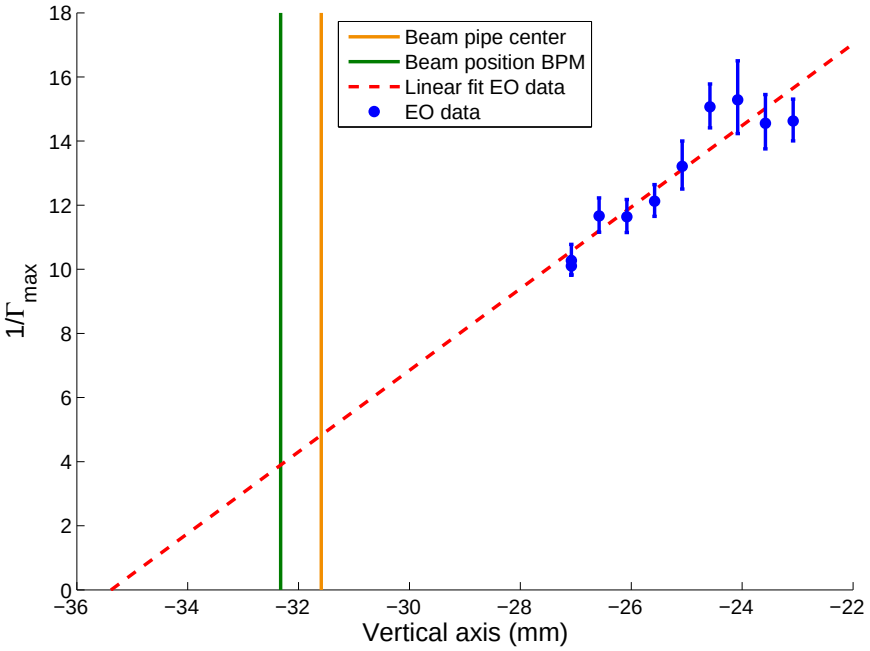

Figure 6.2: The inverse of the maxima of phase retardation Γ for different radial distances.

The BPM beam position and the position from the $1/\Gamma$ extrapolation indicate, that the beam loss detected at $-27\,\mathrm{mm}$ is caused rather by the beam halo than by touching the edge of the beam itself. The standard deviation of the Gaussian radial charge distribution of the beam at the position of the EO monitor is of the order of $1\,\mathrm{mm}$. This would mean that the position of the laser beam during safe operation of the monitor is about $8\,\mathrm{mm}$ from the electron beam center.

6.3 Charge Dependence of the EO Signal

The bunch charge in the accelerator can be varied by adjusting the injector laser intensity in the photoinjector. For a systematic study bunches with different charges Q have been produced. The charge measurements have been done with toroid monitors. The bunch charge dependence of the electric field E_{THz} as well as of Γ is expected to be linear (Sec. 2.1).

Figure 6.3 shows the strength of the signal Γ as function of the bunch charge over a wide range of typical bunch charges at FLASH. For each data point 10 spectra have been taken and averaged. Aside from restrictions due to amplitude jitter, the sensitivity of the EO monitor is expected to be sufficient for bunch profile measurements at $Q = 50\,\mathrm{pC}$ or even lower.

The fact that the linear fit does not cross the origin could be caused by either a calibration error of the toroid system or a systematic effect in the EO method, for instance a wrong reference spectrum caused by amplitude instabilities.

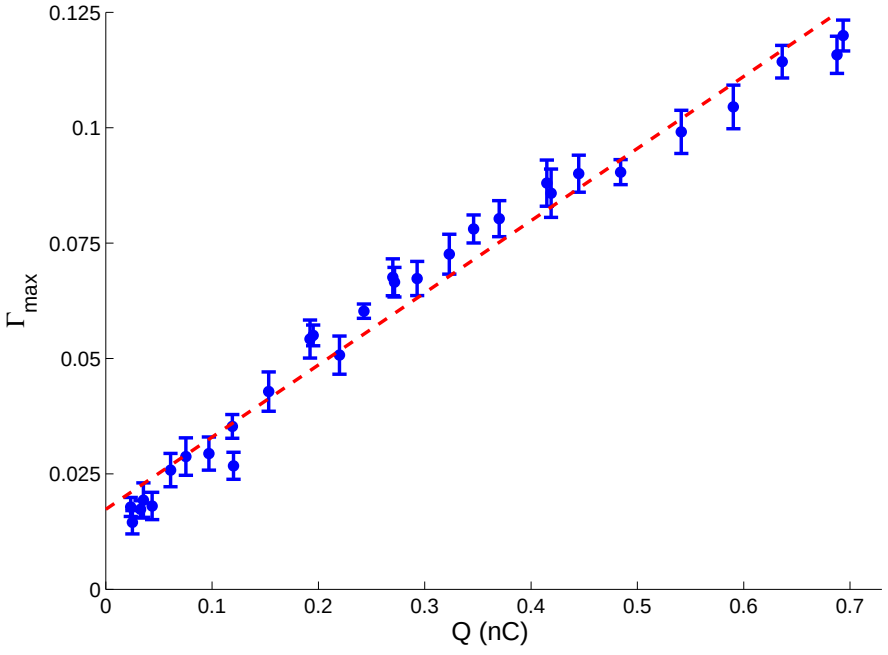

Figure 6.3: Maximum of phase retardation Γ for different electron bunch charges.

6.4 Arrival-Time Measurements

The bunch arrival-time monitors (BAM) are part of the optical synchronization system at FLASH. The BAM is based on the electro-optic effect, measuring the arrival-time of electron bunches based on pick-up electrodes detecting the wake field of the bunch. The transient electrical signal is used to modulate a single pulse out of the pulse train, delivered by the optical master laser oscillator, using an electro-optic fiber-coupled modulator. The steep slope of the transient signal close to its zero crossing allows time resolutions in the order a few femtoseconds [23].

For systematic arrival-time studies the amplitude of the accelerating field in the first accelerating module ACC1 has been varied. The resulting change of electron beam energy effects the length of the path through the bunch compressor BC2 and, therefore, the arrival-time of the electron bunches behind BC2. The BAM 3DBC2 and the EO monitor, both located several meters behind BC2, have been used for simultaneous monitoring. For the EO data the fit algorithm introduced in chapter 5.4 and the time calibration constant have been used for the determination of the arrival-time. Gaussian fits have been applied to an averaged EO signal from 10 single-shots, leading to a statistical uncertainty of the measured arrival-time of less than 20 fs. The precision of the BAM data is in the same order of magnitude but with a single-shot measurement.

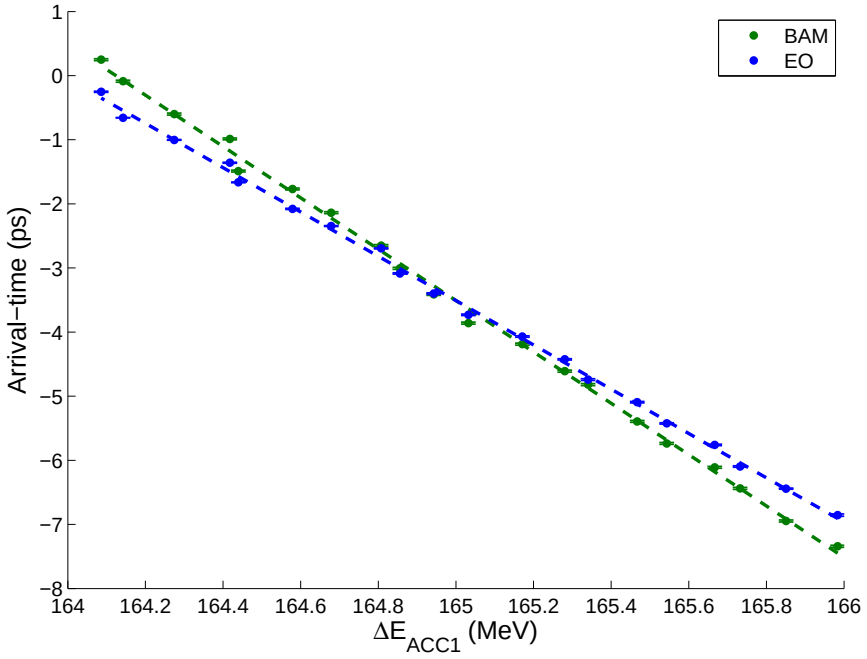

Figure 6.4: Comparative arrival-time measurement, performed with a bunch arrival-time monitor (BAM) and the EO monitor. The change of arrival the time is achieved by a variation of the beam energy and a bunch compressor.

The result of the measurement is shown in figure 6.4). Both monitors show a perfectly linear dependence of the arrival-time on the ACC1 amplitude. With increasing amplitude, the arrival-time becomes smaller, indicating an earlier arrival. The slope of it is $-4.01 \pm 0.04\,\mathrm{ps/MeV}$ for the BAM data and $-3.46 \pm 0.03\,\mathrm{ps/MeV}$ for the EO data. The deviation in the slopes is significantly larger than the statistical uncertainty which is an indicator for a systematic error. Systematic errors on the EO arrival-time measurement, caused by the choice of fit algorithms, are discussed in section 5.4 with the assumption of constant electron beam parameters. As the arrival-time changes observed in this set of data are caused by a passage through a bunch compressor with varying settings of the accelerating structure ACC1, an impact on the longitudinal bunch profile is likely. The bandwidth of the transient signal from the BAM pick-up electrodes is far too low to be sensitive to the longitudinal bunch profile. In consequence, the BAM measures the arrival-time of the centroid of a charge distribution along the longitudinal coordinate [24], whereas the evaluation of the EO signal requires an exact definition of arrival-time that does not dependent on the longitudinal bunch profile.

6.5 Temporal Resolution Limit

For EOSD the relation between the longitudinal coordinate (i.e. temporal coordinate) and the spectral component of the laser pulse is crucial.

In case of an overlap of two electro-magnetic fields, oscillating with frequencies in the THz range, travel through the EO crystal simultaneously. Assuming the central wavelength $\lambda = 1037\,\mathrm{nm}$ of the laser, the corresponding frequency is $f_{\mathrm{las}} \approx 300\,\mathrm{THz}$. The EO effect modulates the electric field of the laser by a frequency determined by the Coulomb field of an electron bunch. The bandwidth depends on the longitudinal charge distribution and contains frequencies $f_{\mathrm{THz}} \geq 1\,\mathrm{THz}$ for compressed bunches behind BC2.
Regardless of f_{THz} mixing frequencies $f_{\mathrm{las}} \pm f_{\mathrm{THz}}$ are created in case of a modulation, adding spectral components to the laser pulse. For higher f_{THz} the wavelength difference of the spectral component added increases, leading to a more distinct distortion of the EO signal due the distortion in the spectrum-time relation. The minimal length of an electron bunch that can be resolved by EOSD without significant distortions T_{lim} can be estimated using [25], [26]

$$T_{\mathrm{lim}} \approx 2.6\ \sqrt{T_0 T_{\mathrm{C}}}\ . \tag{6.2}$$

With the parameters determined in section 4.1.3, $T_0 = 43\,\mathrm{fs}$ and $T_{\mathrm{C}} = 7.2\,\mathrm{ps}$, this yields

$$T_{\mathrm{lim}} \approx 1.4\,\mathrm{ps}\ . \tag{6.3}$$

T_{lim} must be interpreted as the FWHM of the steepest feature in the longitudinal charge profile. T_0 is determined by the spectral bandwidth of the utilized laser and can not be modified whereas the amount of chirp leading to T_{C} can be chosen arbitrarily. The fact that T_{lim} is proportional to the square root of T_{C}, whereas the temporal range is proportional to T_{C} shows that the EOSD detection method is beneficial for bunch lengths in the picosecond range.

To determine the temporal resolution limit of the EO monitor, signals for different states of bunch compressions have been taken (Fig. 6.5a). Measurements have been done for four sets of Φ_{ACC1} and Φ_{ACC39}, the parameters $\Delta E_{\mathrm{ACC1}} = 165\,\mathrm{MeV}$ and $\Delta E_{\mathrm{ACC39}} = 18\,\mathrm{MeV}$ have been kept constant.

The signal taken at lowest compression is shown in orange. The EO signal taken at next higher compression (green) is characterized by a steeper slope in the leading spike, which is resolved by the EO technique with an approx. 1 ps FWHM. There is a tendency of oscillations caused by frequency mixing. For even higher compression, frequency mixing dominates the EO signal, causing signal broadening. The temporal resolution limit is reached. The oscillations before 2 ps for the blue and red curve are a strong evidence for distortions of the spectrum-time relation because they appear to be at earlier times than the arrival-time of the electron bunch.

For a better understanding of the temporal resolution resulting from frequency mixing in relation to the longitudinal bunch profile, simulations on the EOSD process have been done [18], [27]. The simulations assume a Gaussian laser pulse with the properties, discussed in chapter 4.1. Figure 6.5b shows the result of the simulated EOSD process, using Gaussian longitudinal charge distributions for the electron bunches. Except for the asymmetry caused by the asymetric bunch profile that is typical for the set of parameters ΔE and Φ used in ACC1 and ACC39 in figure 6.5a, the simulation reproduces the EO signal including the effects of frequency mixing quite well.

6.6 Longitudinal Bunch Profiles

The transverse deflecting structure (TDS), called LOLA at FLASH, is a well-established diagnostic tool for longitudinal phase space measurements [28], [3]. It is located at the end of the electron linear accelerator, more that 100 m away from the EO monitor in downstream direction (Fig. 1.1). For comparative studies a special setting in the FLASH linac has to be chosen to minimize the effects causing changes of the longitudinal phase space of the electron bunches. This includes a straight path through the bunch compressor BC3 and an on-crest acceleration in the following accelerating modules. The electron beam energy has been increased from about 150 MeV to over 700 MeV because the beam optics is adapted to energies in this range. The dogleg between the EO monitor and the TDS can not be avoided.

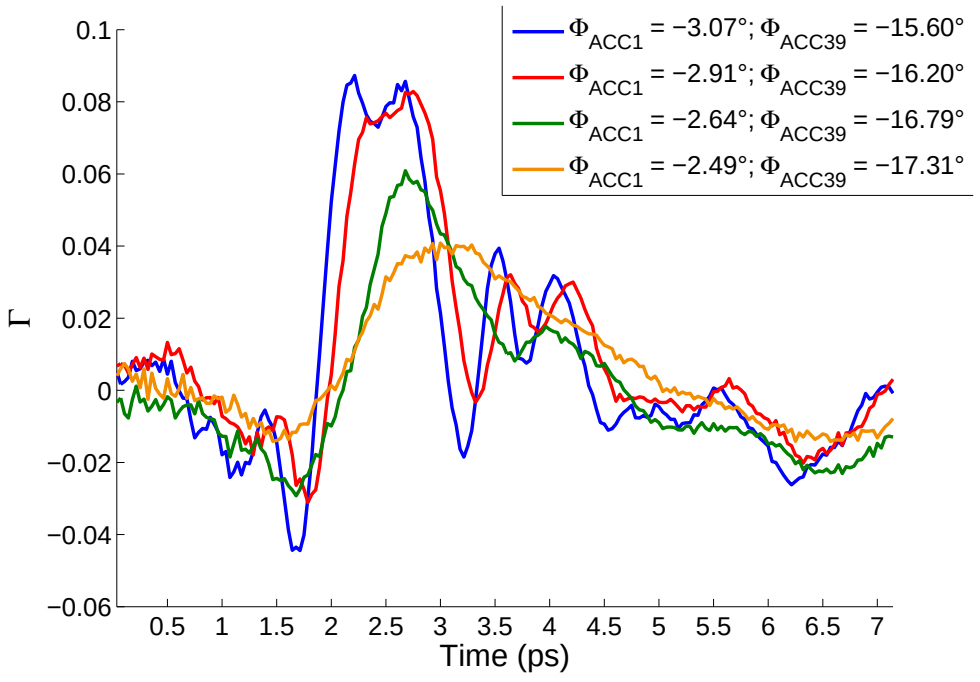

(a)

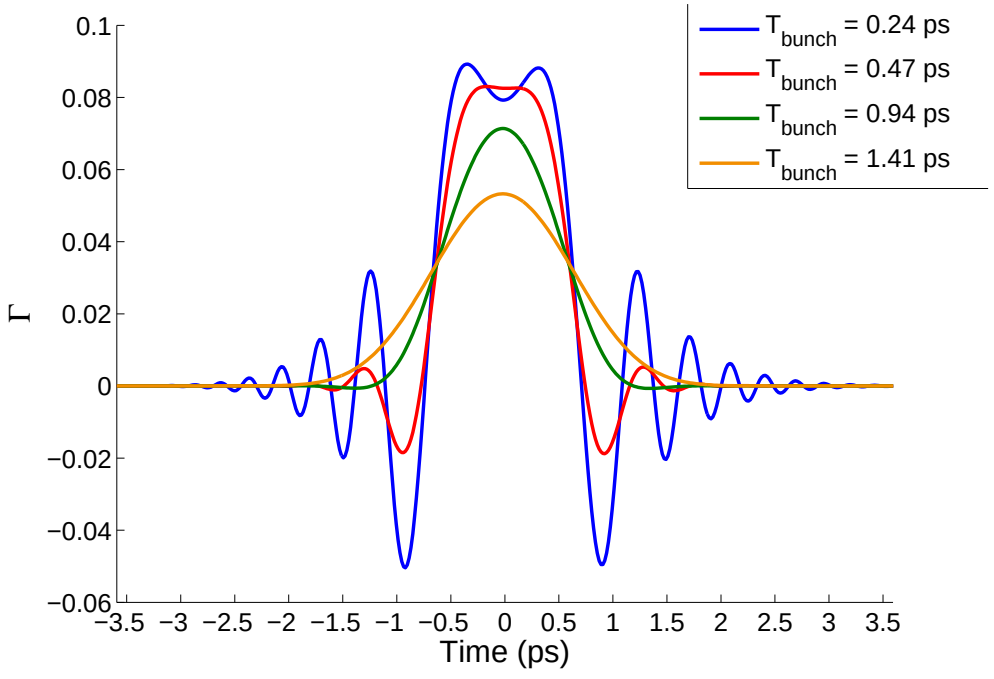

(b)

Figure 6.5: EO signals measured for different bunch compressions (a). Effects of signal distortion due to frequency mixing increase from lower (orange) to higher compression (blue). Simulations of the EOSD effect (b), based on Gaussian shaped electron bunches of different FWHM pulse lengths T_{bunch}.

Longitudinal bunch profiles have been measured simultaneously by the TDS and the EO monitor for five different machine settings. The phase in the first accelerating module has been set to $\Phi_{\mathrm{ACC1}} = 4^\circ$ off-crest. The third harmonic module has been set to $\Phi_{\mathrm{ACC39}} = 12^\circ$ off-crest (decelerating) and the accelerating field in the third harmonic system has been varied ($\Delta E_{\mathrm{ACC39}} = 4...20\,\mathrm{MeV}$) in five steps. The energy loss in ACC39 has been compensated with ACC1. Using the longitudinal bunch profiles measured with the TDS as input, simulations of the EOSD process have been done.

The effect on the bunch compression shows a good agreement between the data taken with the TDS and the EO monitor (Fig. 6.6). With an decreasing phase space linearization in ACC39 a steeper leading edge and a linear decay at the tail is expected. This is reproduced by the TDS (green) and EO (blue) in figures 6.6a, 6.6b and 6.6d. Further decreasing of $\Delta E_{\mathrm{ACC39}}$ leads to a spike in the charge density, measured with the TDS in figures 6.6d and 6.6e. In the EO signal a high-frequent modulation can be observed, because the EO signal is distorted by frequency mixing as the bunch profiles become steeper.

A significant deviation of the measured bunch length can be observed in figure 6.6a. The EO data indicates a shorter bunch than the TDS data whereas the opposite is obtained in all other measurements. A likely reason is the change of the longitudinal phase space during the drift between both diagnostics tools. The dogleg mentioned before leads to a slight decompression due to the energy chirp applied in ACC1 and ACC39. Furthermore, wakefields might have an influence on the electron energy in the tail of the bunch, causing unpredictable effects on the longitudinal bunch profile in the dogleg.

When comparing the figures 6.6d and 6.6e, the signal distortion due to frequency mixing and signal broadening are increased in the measured EO signal whereas the simulated EO signal is nearly unchanged. That might be caused by the fact that the resolution limit of the TDS is reached and the leading slope of the measured bunch profile is resolution limited. The resolution of the TDS depends among others on the imaged temporal range. The electron bunch lengths detected are exceptionally high for this device. Therefore, the TDS resolution of 300 fs to 350 fs for the presented data is comparatively low.

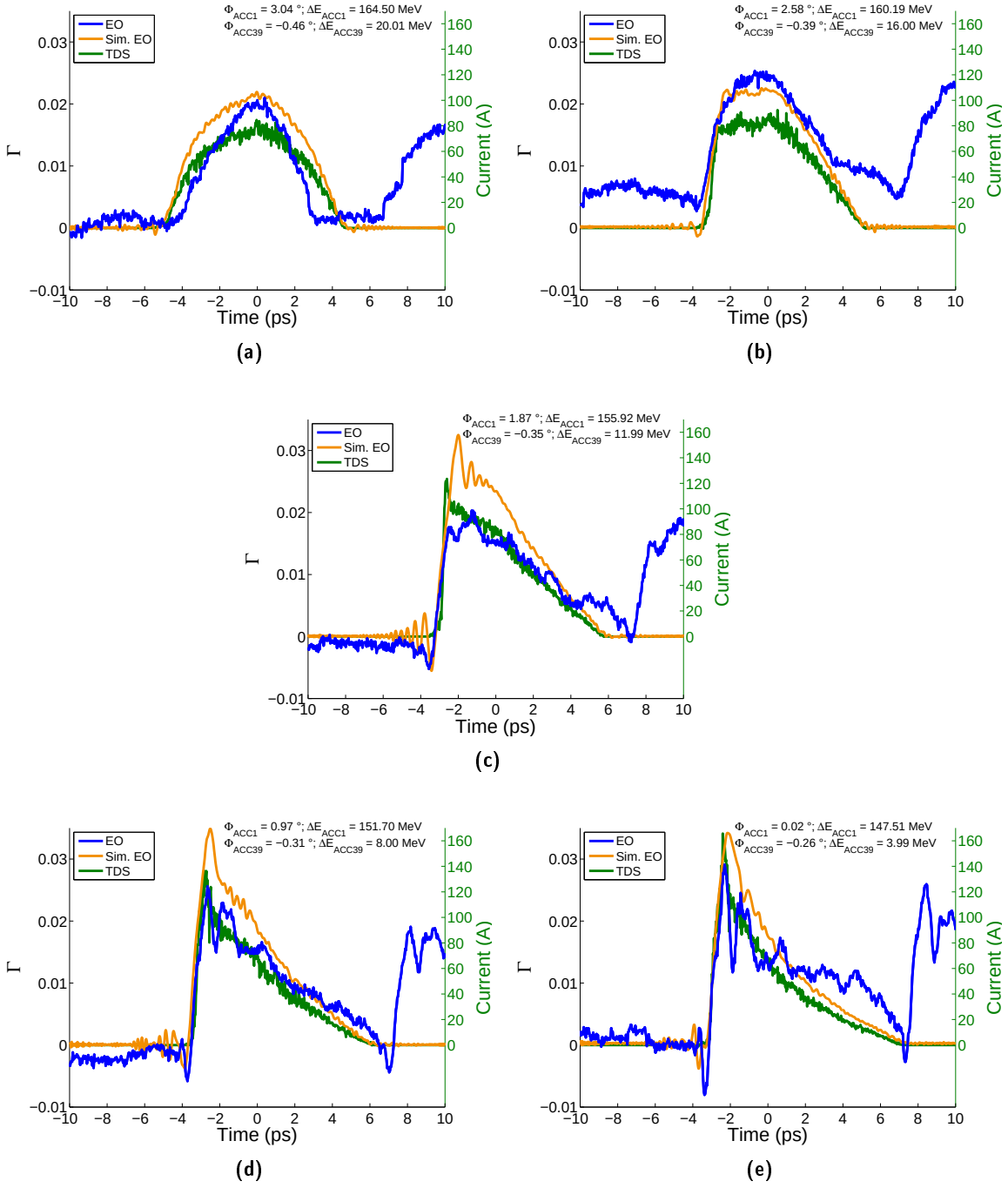

Figure 6.6: Comparison of longitudinal bunch profiles measured with TDS (green) and EOSD (blue) and EOSD simulation data (orange), based on TDS measurements, for different longitudinal bunch shapes.

Conclusions

In this thesis a monitor for longitudinal bunch diagnostics has been commissioned. It utilizes the electro-optic spectral decoding (EOSD) method, providing a single-shot non-destructive detection for permanent beam diagnostics. Electro-optic diagnostic devices based on this prototype are projected to be installed in the European XFEL.

In the first phase of commissioning the experimental setup has been assembled and characterized. A commercial ytterbium fiber laser has been synchronized to the accelerator master oscillator, achieving a permanent lock over weeks with deviations in the order of 60 fs. The entire monitor system has been installed in the accelerator tunnel. It is integrated into the local infrastructure and can be controlled completely by remote access. A two-step method for finding the temporal overlap between the electron bunch and the laser pulse has been developed and applied successfully.

EO measurements of longitudinal bunch profiles have been carried out, obtaining detailed information about the system performance and its limitations. A study on the bunch charge dependence on the detected signal has shown that the monitor sensitivity is convenient for a wide range of bunch charges typical at FLASH. Bunch profiles containing a charge of less than 100 pC can be detected. The temporal resolution limit of the EO monitor is determined by frequency mixing which is an intrinsic limitation due to the EOSD method. An electron bunch of about 1.4 ps FWHM can be detected without significant signal distortion due to frequency mixing. The resolution limit has been approved with simulations. The temporal range of the monitor is 6.4 ps.

First comparative studies have been performed. Arrival-time measurements done with the EO monitor have been compared to data taken by the dedicated bunch arrival-time monitor (BAM) system. A good agreement between the measured data has been observed. A comparative study with the EO monitor and the transverse deflecting structure (TDS) has demonstrated that the EO monitor is an appropriate device for longitudinal bunch profile measurements behind the first bunch compressor in the FLASH accelerator.

The monitor system has proven a high reliability and robustness. For a period of three months no on-site maintenance works have been done. During that time the greater part of the presented measurements has been performed.

Outlook

The EO monitor will be available in the near future. A software tool is in preparation which will automate the control of the EO monitor to a great extend. That is a requirement for an every day use by the accelerator operation crew.

The system performance can be increased by a stabilization of the optical gating. This will reduce the observed amplitude jitter and, therefore, the signal-to-noise ratio. To increase the signal amplitude, a thicker EO crystal can be installed. The signal amplitude grows linearly with the crystal thickness. Both modifications are projected for the next machine shut-down.

For an adjustment of the laser pulse length a grating compressor can be integrated into a modified version of the EO front end. With a variable chirp the ratio between the usable range and the temporal resolution of the monitor can be adapted to the electron bunch length and the monitor may become usable for the EO sampling detection scheme.

The integrated design of the EO front end as well as the infrastructure inside the accelerator tunnel have proved to be reliable. Thus, the operation of the monitor for bunch detection in the European XFEL becomes feasible.

Appendices

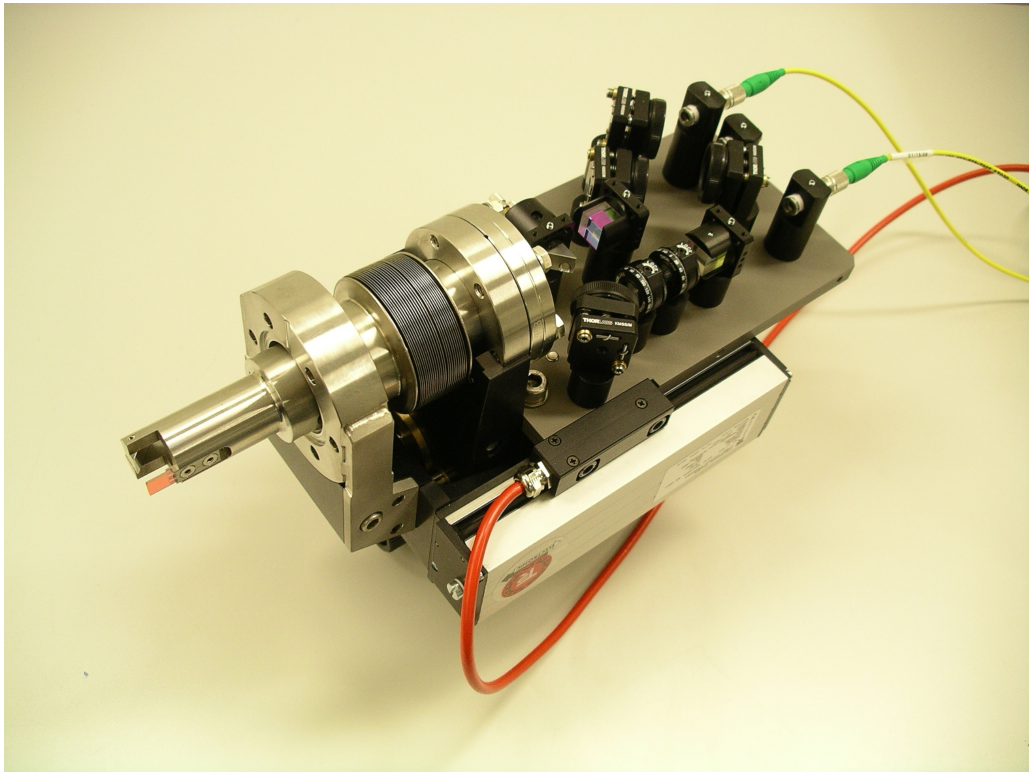

Figure A.1: Photograph of an EO front end in the cleanroom and with retarder attachments for manual adjustment. For the setup utilized both retarders are motorized. By courtesy of B. Steffen.

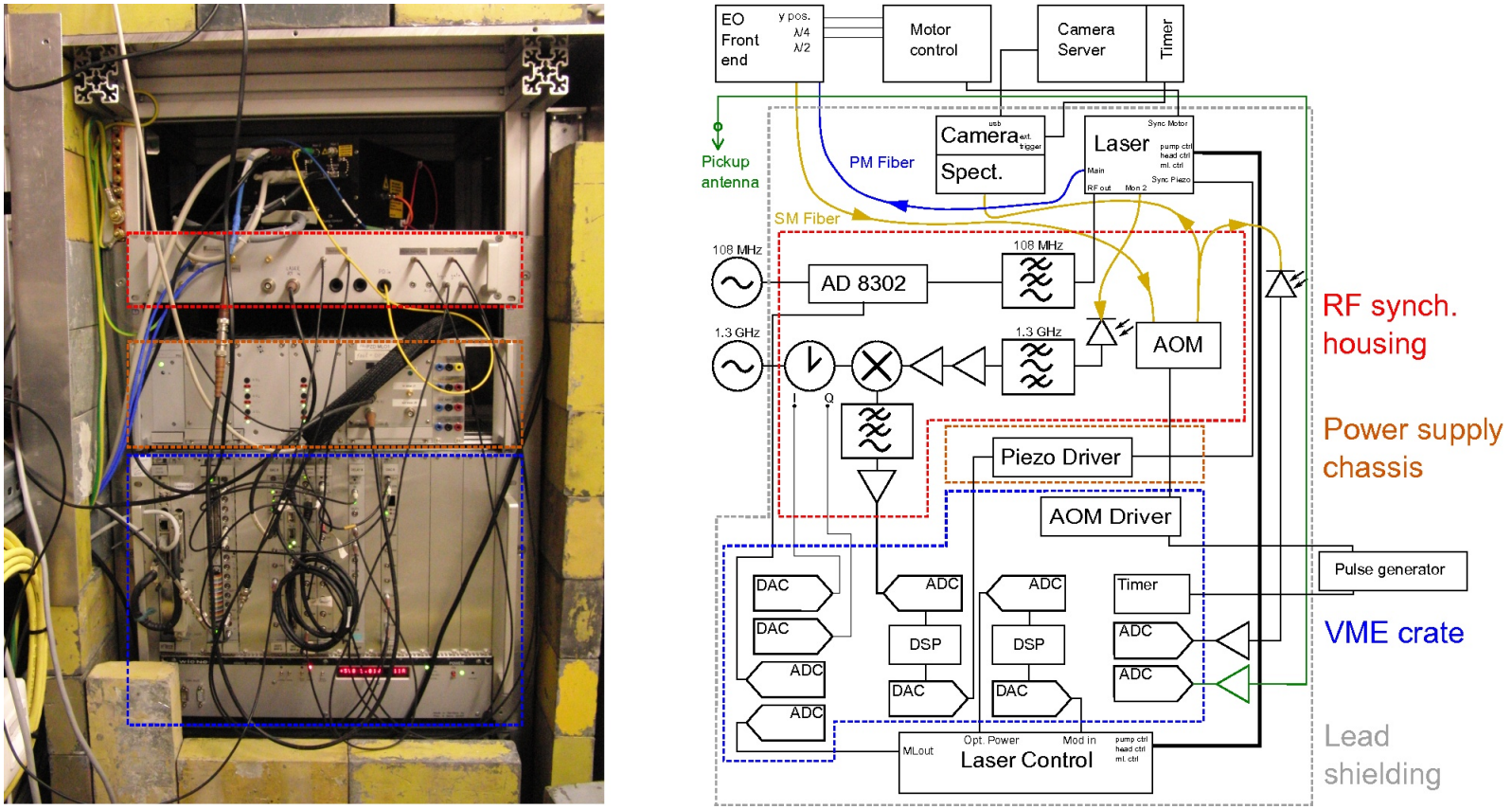

Figure A.2: Photograph and schematic of the lead shielded electronics rack in the accelerator tunnel. The crate is 1.1 m high. The laser is placed on top of the 19-inch housing (red). The spectrometer unit (not yet installed when the picture had been taken) is installed next to the laser. A power supply unit (orange) and the VME crate (blue) are installed below. The laser control unit (covered by lead bricks in this picture) is placed on the concrete floor. The pickup antenna, cable and amplifier are shown in green in the schematic.

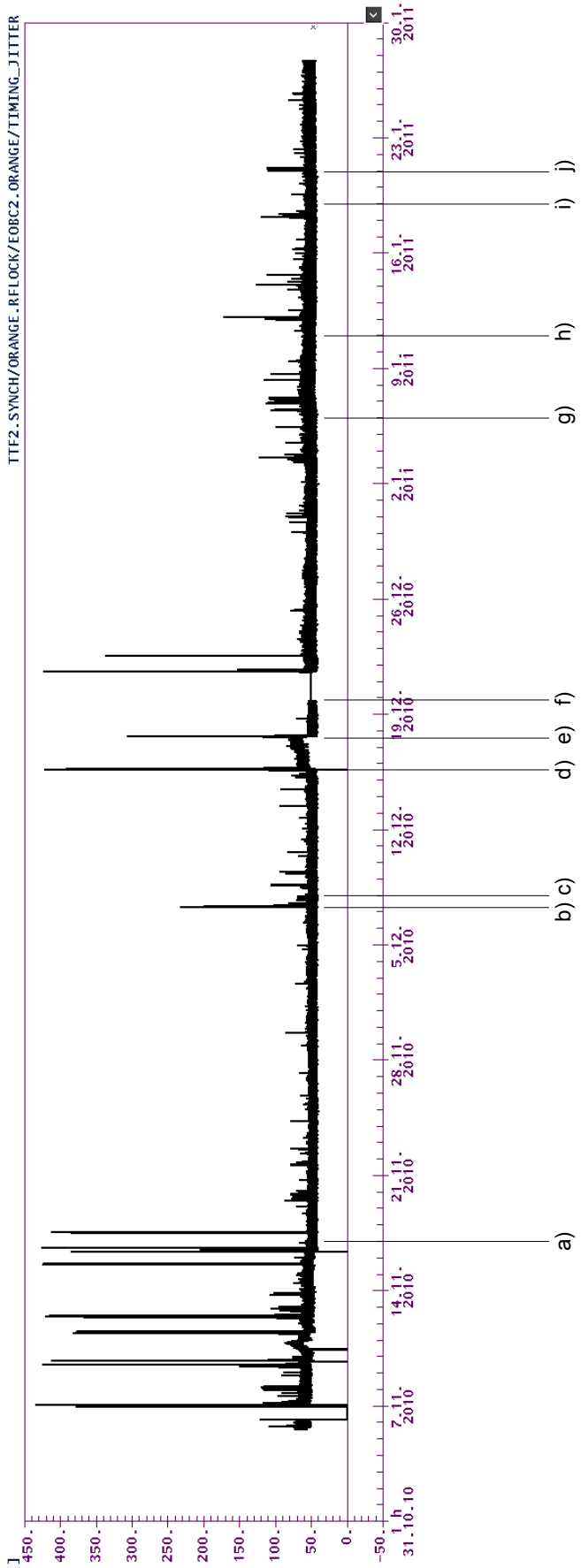
TTF2.SYNCH/ORANGE.RFLOCK/EOBC2.ORANGE/TIMING_JITTER
[]
450.
400.
350.
300.
250.
200.
150.
100.
50.
0.
-50.
1 h
31.10.10
7.11.
2010
14.11.
2010
21.11.
2010
28.11.
2010
5.12.
2010
12.12.
2010
19.12.
2010
26.12.
2010
2.1.
2011
9.1.
2011
16.1.
2011
23.1.
2011
30.1.
2011
a)
b) c)
d)
e)
f)
g)
h)
i)
j)

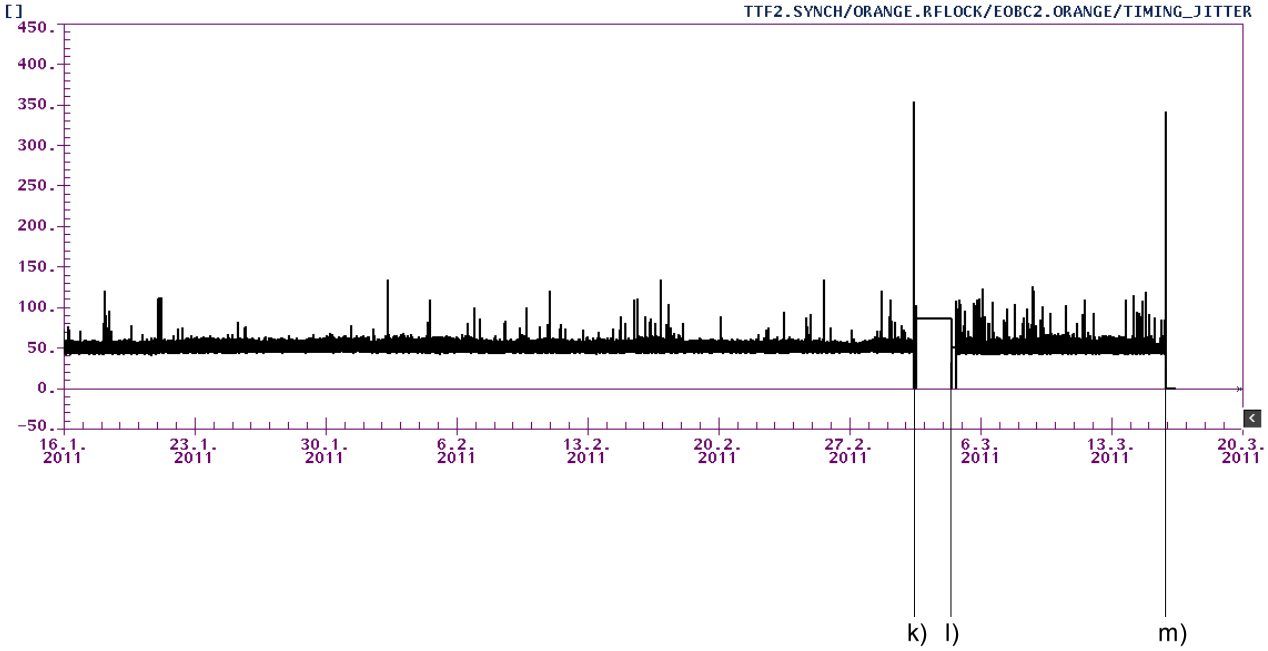

Figure A.3: The in-loop jitter of the laser synchronization in fs versus the time. The data has been recorded by the FLASH control system, covering more than four months. a) Long time monitoring performed.(Fig. 4.5), b) Maintenance works. c) First overlap established. d), e) Laser mode-lock studies. f) Projected power cutoff. i) The author's birthday. g), h), j) Studies on the EO monitor during dedicated beam time. k), l), m) RF Synchronization break due to automation software tests.

Acronyms

a.u.	arbitrary units
ACC	accelerating structure
ACF	autocorrelation function
ADC	analog-to-digital converter
AOM	acousto-optic modulator
BAM	bunch arrival-time monitor
BBO	beta-barium borate
BC	bunch compressor
BCM	bunch compression monitor
BPM	beam position monitor
CCD	charge-coupled device
CDR	coherent diffraction radiation
CTR	coherent transition radiation
DAC	digital-to-analog converter
DC	direct current
DSP	digital signal processor
EO	electro-optic
EOS	electro-optic sampling
EOSD	electro-optic spectral decoding
EOTD	electro-optic temporal decoding
FC/APC	ferrule connector with angled physical contact
FEL	free-electron laser
FLASH	Free-Electron Laser in Hamburg
FWHM	full width at half maximum
GaP	gallium phosphide
GVD	group velocity dispersion
HHG	high-harmonic generation
InGaAs	indium gallium arsenide
MO	master oscillator
OTR	optical transition radiation
PM	polarization-maintaining (optical fiber)
PSI	Paul Scherrer Institut
RF	radio frequency
RMS	root mean square

SASE	self-amplified spontaneous emission
SFG	sum-frequency generation
SHG	second-harmonic generation
SM	single-mode (optical fiber)
SSA	signal source analyzer
SSB	single-sideband
TDS	transverse deflecting structure
TEM	transverse electro-magnetic
TESLA	teraelectronvolt energy superconducting linear accelerator
TTF	TESLA test facility
UV	ultraviolet
VM	vector modulator
VME	Versa Module Eurocard
VUV	vacuum ultraviolet

Bibliography

[1] U. Happek, A. J. Sievers and E. B. Blum: *Observation of Coherent Transition Radiation.* Phys. Rev. Lett., 67(21):2962–2965, Nov 1991.

[2] M. Castellano, V. A. Verzilov, L. Catani, A. Cianchi, G. Orlandi and M. Geitz: *Measurements of Coherent Diffraction Radiation and its Application for Bunch Length Diagnostics in Particle Accelerators.* Phys. Rev. E, 63(5):056501, Apr 2001.

[3] R. Akre, L. Bentson, P. Emma and P. Krejcik: *Bunch Length Measurements Using a Transverse RF Deflecting Structure in the SLAC Linac.* In *Proceedings of the EPAC 2002*, Paris, France, 2002.

[4] X. Yan, A. M. MacLeod, W. A. Gillespie, G. M. H. Knippels, D. Oepts, A. F. G. van der Meer and W. Seidel: *Subpicosecond Electro-optic Measurement of Relativistic Electron Pulses.* Phys. Rev. Lett., 85(16):3404–3407, Oct 2000.

[5] I. Wilke, A. M. MacLeod, W. A. Gillespie, G. Berden, G. M. H. Knippels and A. F. G. van der Meer: *Single-Shot Electron-Beam Bunch Length Measurements.* Phys. Rev. Lett., 88(12):124801, Mar 2002.

[6] G. Berden, S. P. Jamison, A. M. McLeod, W. A. Gillespie, B. Redlich and A. F. G. van der Meer: *Electro-Optic Technique with Improved Time Resolution for Real-Time, Nondestructive, Single-Shot Measurements of Femtosecond Electron Bunch Profiles.* Phys. Rev. Lett., 93:114802, 2004.

[7] A. Azima and others: *Jitter Measurements by Spatial Electro-Optical Sampling at the FLASH Free Electron Laser.* In *Proceedings of the EPAC 2006*, Edinburgh, Scotland, 2006.

[8] G. Berden, W. A. Gillespie, S. P. Jamison, E.-A. Knabbe, A. M. MacLeod, A. F. G. van der Meer, P. J. Phillips, H. Schlarb, B. Schmidt, P. Schmüser and B. Steffen: *Benchmarking of Electro-Optic Monitors for Femtosecond Electron Bunches.* Phys. Rev. Lett., 99(16):164801, Oct 2007.

[9] P. Schmüser, M. Dohlus and J. Rossbach: *Ultraviolet and Soft X-Ray Free-Electron Lasers.* Springer, 2008.

[10] S. Schreiber, B. Faatz, J. Feldhaus, K. Honkavaara, J. Rossbach, R. Treusch and M. Vogt: *FLASH Upgrade and First Results.* In *Proceedings of the FEL Conference 2010*, Malmö, Sweden, 2010.

[11] B. Aune and others: *Superconducting TESLA Cavities.* Phys. Rev. ST Accel. Beams, 3(9):092001, Sep 2000.

[12] R. Ischebeck: *Transverse Coherence of a VUV Free Electron Laser.* PhD thesis, Universität Hamburg, 2003.

[13] M. Röhrs, C. Gerth, H. Schlarb, B. Schmidt and P. Schmüser: *Time-resolved Electron Beam Phase Space Tomography at a Soft X-ray Free-Electron Laser.* Phys. Rev. ST Accel. Beams, 12(5):050704, May 2009.

[14] C. Behrens, D. Nicoletti, B. Schmidt and S. Wesch: *Upgrade and Evaluation of the Bunch Compression Monitor at the Free-Electron Laser in Hamburg (FLASH).* In *Proceedings of the IPAC 2010*, Kyoto, Japan, 2010.

[15] S. Wesch. private communication, 2011.

[16] S. Casalbuoni, B. Schmidt, P. Schmüser, V. Arsov and S. Wesch: *Ultrabroadband Terahertz Source and Beamline Based on Coherent Transition Radiation.* Phys. Rev. ST Accel. Beams, 12(3):030705, Mar 2009.

[17] J. D. Jackson: *Classical Electrodynamics.* John Wiley and Sons, Inc., 3rd edition, 1999.

[18] S. Casalbuoni, H. Schlarb, B. Schmidt, P. Schmüser, B. Steffen and A. Winter: *Numerical Studies on the Electro-Optic Detection of Femtosecond Electron Bunches.* Phys. Rev. ST Accel. Beams, 11(7):072802, Jul 2008.

[19] B. Steffen: *Electro-Optic Methods for Longitudinal Bunch Diagnostics at FLASH.* PhD thesis, Universität Hamburg, 2007.

[20] G. P. Agrawal: *Nonlinear Fiber Optics.* Elsevier Inc., 4th edition, 2007.

[21] H. Redlin, A. Al-Shemmary, A. Azima, N. Stojanovic, F. Tavella, I. Will and S. Düsterer: *The FLASH Pump-Probe Laser System: Setup, Characterization and Optical Beamlines.* Nuclear Instruments and Methods in Physics Research Section A: Accelerators, Spectrometers, Detectors and Associated Equipment, 635(1, Supplement 1):S88 – S93, 2011. PhotonDiag 2010.

[22] H. Lim, F. O. Ilday and F. W. Wise: *Generation of 2-nJ Pulses from a Femtosecond Ytterbium Fiber Laser.* Opt. Letters, 28(8):660–662, 2003.

[23] M. K. Bock, M. Felber, P. Gessler, K. E. Hacker, F. Loehl, F. Ludwig, H. Schlarb, B. Schmidt, J. Zemella, S. Schulz and L.-G. Wissmann: *Recent Developments of the Bunch Arrival Time Monitor with Femtosecond Resolution at FLASH.* In *Proceedings of the IPAC 2010*, Kyoto, Japan, 2010.

[24] F. Löhl: *Optical Synchronization of a Free-Electron Laser with Femtosecond Precision.* PhD thesis, Universität Hamburg, 2009.

[25] J. Fletcher: *Distortion and Uncertainty in Chirped Pulse THz Spectrometers.* Opt. Express, 10(24):1425–1430, 2002.

[26] S. Jamison and others: *Femtosecond Resolution Bunch Profile Measurements.* In *Proceedings of the EPAC 2006*, Edinburgh, Scotland, 2006.

[27] B. Steffen. private communication, 2011.

[28] C. Behrens and C. Gerth: *On the Limitations of Longitudinal Phase Space Measurements Using a Transverse Deflecting Structure.* In *Proceedings of the DIPAC 2009*, Basel, Switzerland, 2009.

Acknowledgments

Diese Arbeit entstand mit Hilfe vieler Menschen sowohl am DESY als auch in der übrigen Welt. Dafür möchte ich meinen herzlichen Dank aussprechen.

Zunächst möchte Herrn Dr. Bernhard Schmidt für die freundlichen Aufnahme in die Arbeitsgruppe FLA danken. Die Diskussionen mit ihm und seine Ratschläge und konstruktiven Kritiken waren mir von großem Nutzen und brachten meine Arbeit voran.

Herr Prof. Dr. Jörg Roßbach weckte mein Interesse für die Beschleunigerphysik während meines Studiums. Er vermittelte mir diese Diplomarbeitsstelle und ist Gutachter dieser Arbeit. Dafür möchte ich mich bedanken.

Laurens als mein direkter Vorgesetzter und Bürokollege half mir in unzähligen Belangen rund um meine Diplomarbeit. Dazu zählen sowohl Arbeiten im Laserlabor als auch das Windschattenspenden auf der Fahrt zur Konferenz.

Die Zusammenarbeit mit Bernd bei Arbeiten am Meßaufbau und seine Unterstützung bei der Bedienung der großen Maschine während der Meßschichten trugen maßgeblich zu dieser Arbeit bei.

Für die angenehme Arbeitsatmosphäre vielen Dank an Marie, Minjie, Sebastian, Stephan, Christopher, Uschi, Ingrid, Ernst-Axel und Herbert. An dieser Stelle möchte ich auch die Gruppennachbarn Holger, Matthias, Patrick und Thorsten dankend erwähnen.

Die Beschleunigerphysikgruppe der Universität Hamburg veranstaltete regelmäßig Seminare mit interessanten Fachvorträgen, die zudem den Freitagnachmittag versüßten.

Albert, Matthias, Karol und Karl-Heinz fertigten etliche größere und kleinere Unikate für mein Projekt an, oft von heute auf morgen und immer passgenau.

Meine Studienzeit mit euch, Vici, Damian, Steffi, Aila, Yasar, Martin, Nadja, Asi, Almut[1], Andrey, Eike, Markus, Jan, Max und Flo, war eine sehr schöne Zeit. Eine solche Fülle unterschiedlicher Charaktere, die gemeinsam die unterschiedlichsten Aktivitäten unternehmen, findet man selten! Ich war dabei und habe es sehr genossen. :-)

Ein Dankeschön geht auch an Kathi, Martin und Sascha für ein gemütliches gemeinsames Wohnen und an Sabine für's gelegentliche abends mal Ausgehen.

Bei meiner Familie, insbesondere bei meinen Großeltern, möchte ich mich für die Unterstützung während meines Studiums ganz herzlich bedanken.

[1] Meine Almut! In meinem Leben weitaus mehr als eine Fußnote!